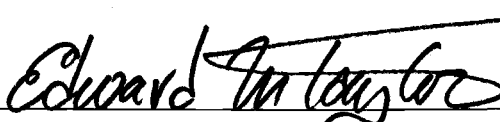


AN ABSTRACT OF THE THESIS OF

Brittain Eames Hill for the degree of Master of Science in  
Geology presented on June 7, 1984.

Title: Petrology of the Bend Pumice and Tumalo Tuff, A Pleistocene  
Cascade Eruption Involving Magma Mixing

Abstract approved: \_\_\_\_\_



Dr. E. M. Taylor

The Bend pumice and Tumalo tuff are products of a plinian eruption which occurred sometime between 0.89 and 2.6 m.y. The Bend pumice is a poorly consolidated, air-fall vitric lapilli tuff, which overlies a zone of reworked tephra. Perlitic obsidian in the reworked zone probably represents the remains of a dome which filled the eruptive vent and is chemically related to the Bend pumice magma. Detailed grain size analysis of the air-fall part of the Bend pumice shows that the eruptive vent was located approximately 10-20 km west of Bend, Oregon. Grain size variations in vertical section are probably related to fluctuations in the diameter of the vent rather than interruptions in deposition of the Bend pumice.

The Tumalo tuff is a nonwelded to moderately welded ash-flow tuff which directly overlies the Bend pumice. Lack of discernable normal grading in the upper 50 cm of the Bend pumice indicates that the Tumalo tuff was emplaced before the Bend pumice was completely

deposited and leads to the conclusion that the Tumalo tuff is the product of collapse of the Bend pumice eruption column. The Tumalo tuff was formed by one episode of flow and has a well developed basal 2a layer. Variations in the distal character of layer 2a are thought to represent complex flow conditions in the head of the Tumalo tuff ash flow. Mixed pumices also are found in proximal Tumalo tuff deposits.

The Bend pumice and Tumalo tuff are peraluminous and rhyodacitic. Within analytical uncertainties, they have identical major, minor, and trace element abundances. Both contain fresh hornblende in the mineral assemblage Plg + Opx + Mgt + Zr + Ap. The hornblende appears to have been a liquidus phase and indicates that the rhyodacite evolved under high pressure, hydrous conditions. A higher La to Ce ratio and a strong negative Eu anomaly in the B-T rhyodacite further indicates that the Bend pumice and Tumalo tuff evolved under physical conditions quite distinct from other rhyodacites in the central Oregon High Cascades analysed by Hughes (1982).

Mixed pumices in the Tumalo tuff represent the incomplete mixing between Bend-Tumalo rhyodacite and a dacitic magma. Trace element modeling fails to provide an unequivocally common path of crystal fractionation between these two magmas. The magmas can not be directly related through thermogravitational diffusion or assimilation. While mixed pumice formation is usually attributed to mixing of genetically related magmas, Tumalo tuff mixed pumices were produced through the mixing of genetically unrelated magmas.

Petrology of the Bend Pumice and Tumalo Tuff,  
A Pleistocene Cascade Eruption Involving Magma Mixing

by

Brittain Eames Hill

A THESIS  
submitted to  
Oregon State University

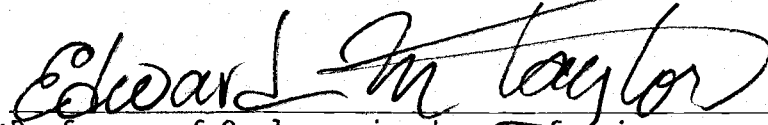
in partial fulfillment of  
the requirements for the  
degree of

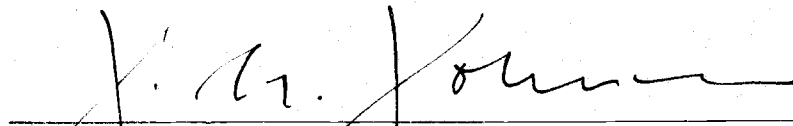
Master of Science

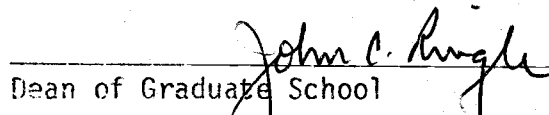
Completed June 7, 1984

Commencement June 1985

APPROVED:

  
\_\_\_\_\_  
Professor of Geology, in charge of major

  
\_\_\_\_\_  
Acting Head of Department of Geology

  
\_\_\_\_\_  
Dean of Graduate School

Date thesis is presented June 7, 1984

Typed by Brittain E. Hill

## ACKNOWLEDGEMENTS

I would like to thank Dr. E. M. Taylor for his continuous support and guidance throughout this thesis and for his ability to remain unperturbed at even the most outlandish of interpretations. I am likewise indebted to Dr. R. A. Schmitt for his instruction at the OSU Radiation Center and for signing all those irradiation requests. Thanks are also given to Dr. E. J. Dasch for his input and review of this thesis, to Dr. W. H. Taubeneck for many hours of patient mineralogical explanations, and Dr. L. W. Snee for his continuous encouragement.

Many others have contributed to the development of this thesis; Dr. Scott Hughes was indispensable in helping with the INAA and in supplying sundry geochemical thoughts. Soon-to-be-Dr. Gary Smith's aid in finding mixed pumices cannot be forgotten, nor can his uncanny ability to find the previously unobserved in the field go without thanks. Special thanks are also given to the rest of the Deschutes Group: Rich Conrey, Tom Dill, Angela McDannel, Dave Wendland, and Gene Yogodzinski. Larry Chitwood, U.S.F.S. Bend, provided many valuable insights into the Bend pumice and Tumalo tuff, and generously allowed me access to his unpublished maps of the southern part of the thesis area. I thank Mr. W. Miller of Central Oregon Pumice Co, Mr. C. Clark of Cascade Pumice Co., and Mr. D. Coats of Coats Construction Co. for permission to map and collect samples on their property.

This thesis was supported in part by a \$200 Sigma Xi Grant-in-aid-of Research. Research support made available by the OSU Radiation Center and Milne Computer Center was indispensable to the completion of this thesis.

Finally, I dedicate this thesis to my fiancée, Ute Kehl and to my parents. Without their unfailing encouragement and support over these last three years, this thesis would not have been possible.

## TABLE OF CONTENTS

1 INTRODUCTION	1
1.1 Location and Accessibility	1
1.2 Previous Work	3
1.3 Central Oregon Cascade Geology	4
1.4 Magma Mixing and Mixed Pumices	8
1.5 Research Methods	9
2 THE BEND PUMICE	15
2.1 Lower Reworked Zone	15
2.2 Upper Air-Fall Zone	19
2.3 Grain Size Analysis	23
3 THE TUMALO TUFF	33
3.1 Layer 1(P) Deposits	33
3.2 Basal Layer 2a	35
3.3 Main Nonsorted Layer 2b	44
3.4 Post Emplacement Effects	48
4 MINERALOGY	53
4.1 Plagioclase	53
4.2 Pyroxenes	54
4.3 Amphibole	55
4.4 Olivine	57
4.5 Oxides and Accessory Phases	57
5 GEOCHEMISTRY	60
5.1 General Concepts	60
5.2 Bend Pumice Geochemistry	63
5.3 Tumalo Tuff Geochemistry	69
5.4 Mixed Pumice Geochemistry	72
SUMMARY AND CONCLUSIONS	81
REFERENCES	85

## TABLE OF CONTENTS cont.

### APPENDICES

Appendix 1: Mineral / melt distribution coefficients used in geochemical modeling.	91
Appendix 2: C-1 chondrite elemental abundances.	92
Appendix 3: Bend pumice geochemistry and sample locations.	93
Appendix 4: Tumalo tuff geochemistry and sample locations.	97



## LIST OF FIGURES

Figure	Page
1: Index map of the thesis area	2
2: Index map showing general features of the central High Cascades of Oregon	5
3: Stratigraphic column of the thesis area, modified from Peterson et al. (1976) and Taylor (1980)	7
4: Simplified geologic map of the Bend pumice and Tumalo tuff, showing major faults and sample location sites	10
5: Generalized geologic map of the Bend pumice and Tumalo tuff, showing locations active and abandoned pumice quarries, and recognisable exposures of Bend pumice lower reworked zone	16
6: Lower reworked zone of the Bend pumice	18
7: Typical section of the Bend pumice upper air-fall zone	21
8: Bend pumice subsurface isopach map from water well-log data	22
9: Cumulative frequency curves for Bend pumice sections located at Deschutes River Ranch (9102) and Tumalo State Park (9101)	26
10: Cumulative frequency curves for Bend pumice sections located at Laidlaw Butte (9111) and west of Bend, Oregon (9113)	27
11: Isomedian map for the Bend pumice, using median grain-size diameters from the upper 10-50 cm of the deposit	30
12: Median grain size vs. distance from 3 possible vent locations, with exponential best-fit curves	32
13: Proximal features of the Tumalo tuff, including layer 1(P)	34
14: Cumulative frequency curves for two Tumalo tuff sections, contrasting layers 2a and 2b	38
15: Layer of coarse pumice within the basal layer 2a of the Tumalo tuff	40

# LIST OF FIGURES cont.

Figure	page
16: Multiple reverse-graded units within layer 2a of the Tumalo tuff, exposed in an abandoned pumice quarry south-east of Tumalo State Park	41
17: Coarsening and thickening in 2a layer of the Tumalo tuff in response to a declivity in the Bend pumice, approximately 20 m south from figure 16	42
18: Diagram of possible flow conditions in the base of the distal Tumalo ash flow	43
19: Tumalo tuff mixed pumice	46
20: Simplified geologic map of the Bend pumice and Tumalo tuff, showing the distribution of welded Tumalo tuff	50
21: $\text{FeO} - \text{TiO}_2 - \text{Fe}_2\text{O}_3$ diagram modified from Buddington and Lindsley (1964)	58
22: Mineral / Melt distribution coefficients used in geochemical models	62
23: Chondrite normalized plot of selected Bend pumice samples	66
24: Chondrite normalized plot of the average of 7 Tumalo tuff rhyodacite pumice zones and the average of 7 dacitic pumice zones from the Tumalo Tuff mixed pumices	74

## LIST OF TABLES

Table	Page
1: Bend pumice grain size weight percentages	25
2: Tumalo tuff grain size weight percentages	37
3: Bend pumice chemical abundances and C.I.P.W. normative mineralogies	64
4: Tumalo tuff chemical abundances	70

## LIST OF PLATES

1: Geologic map of the Bend pumice and Tumalo tuff, including contact geology	in map pocket
---	---------------

PETROLOGY OF THE BEND PUMICE AND TUMALO TUFF,  
A PLEISTOCENE CASCADE ERUPTION INVOLVING MAGMA MIXING

INTRODUCTION

A large Plinian eruption occurred in the central Oregon High Cascades about 1 to 2 million years ago. The eruption produced the air-fall Bend pumice and ash-flow Tumalo tuff, two deposits which are well exposed throughout the Bend area. The age, source, and evolution of these units are the subjects of this study. Some pumices in the Tumalo tuff preserve incomplete mixing between two distinct magmas. Mixed pumices are a common feature of Cascade volcanism but their importance has not been commensurate with their investigation. The possible origins of the contrasting magmas represented by the Tumalo tuff mixed pumices are also considered in this thesis.

1.1 Location and Accessibility

The thesis area lies in an area of approximately 150 square miles around Bend, Oregon and is shown in figure 1. The area includes parts of the Tumalo Dam, Tumalo, Shevlin Park, Bend, Benham Falls, and Lava Butte 7 1/2 minute quadrangles and is delimited by  $44^{\circ} 12'$  and  $43^{\circ} 55'$  north latitude,  $121^{\circ} 16'$  and  $121^{\circ} 27'$  west longitude.

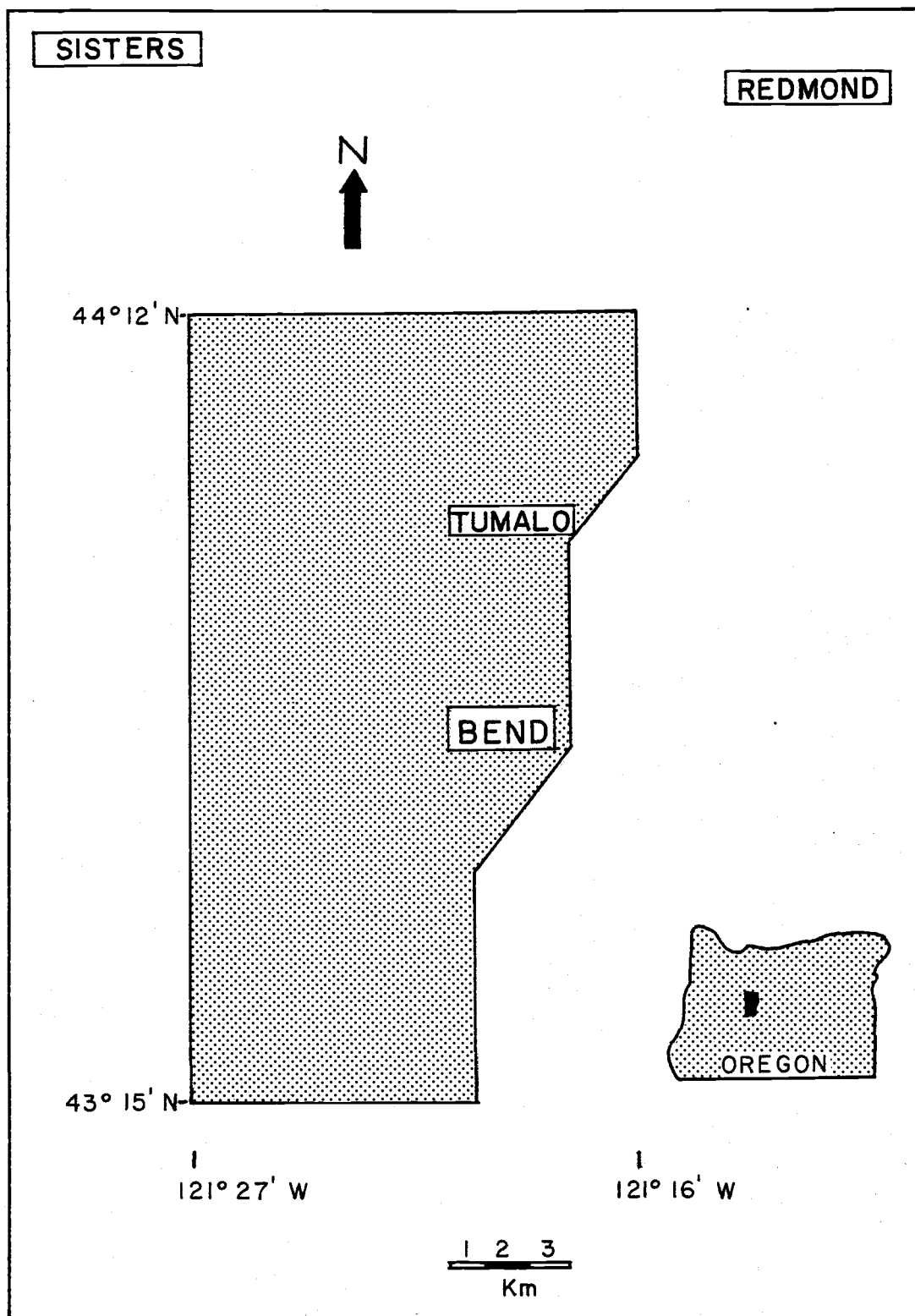


Figure 1: Index map of the thesis area.

The entire area is accessible through a complex network of county, forest service, logging, and mining roads and on several abandoned logging railroad grades. Excellent exposure is provided by numerous active and abandoned pumice quarries throughout the field area. Natural exposures of more than several square meters are limited to active stream courses.

## 1.2 Previous Work

Howell Williams (1957) first mapped and described the geology of the Bend Quadrangle. He described the Bend pumice and Tumalo tuff as "Recent pumice avalanche deposits" of dacitic composition. Peterson, Groh, Taylor, and Stensland (1976) mapped the geology of Deschutes County, which encloses the study area, at a scale of 1:87,500. They mapped the distribution of an all-inclusive Quaternary pyroclastic unit, which included the Bend pumice and Tumalo tuff. Mimura and MacLeod (1978) and Mimura (in press) concluded from air-fall isopachs and ash-flow pumice imbrication that the Bend pumice and Tumalo tuff were erupted from a source south-southwest of Bend. They believed the paleovent could be related to a large (20 mgal) negative Bouger anomaly west of the Newberry volcanic complex. Taylor (1980) first named the white air-fall pumice deposit around Bend the "Bend pumice," and the overlying rhyodacitic ash-flow tuff the "Tumalo tuff." MacLeod, Sherrod, and Chitwood (1982) mapped the distribution of a unit containing "ash-flow tuffs and pumice deposits along the

Deschutes River area", which included the Bend pumice and Tumalo tuff. Their map only describes Bend pumice and Tumalo tuff exposures in the Lava Butte and Benham Falls quadrangles, which comprise the southern quarter of the thesis area. They also concluded that the Bend pumice and Tumalo tuff were erupted from a vent west of Newberry Volcano, approximately 2 m.y.b.p. Hughes (1982) analysed basaltic to rhyodacitic volcanic rocks of the Three Sisters area and summarized the petrogenetic history of the central Oregon High Cascades.

### 1.3 Central Oregon Cascade Geology

During middle to late Miocene, calc-alkaline volcanism on going along an arc coincident with the present High Cascade axis (Taylor, 1978). Volcaniclastic and epiclastic material of the Deschutes Formation was deposited to the east of the Cascade arc in the Deschutes Basin (Figure 2), from 7.6 to 4.5 m.y.b.p. (Smith and Snee, 1983). The Deschutes Formation is associated with a period of crustal extension within the central High Cascade arc, which culminated in the formation of a north-to-south trending graben about 4.5 m.y.b.p. (Taylor, 1981). Graben formation was accompanied by a shift to dominately mafic volcanism, which covered the Deschutes Formation source vents and served as a platform for the development of the present High Cascade stratocones.

Paleodrainage orientations in the southern exposures of the Deschutes Formation (Smith and Taylor, 1983) and a

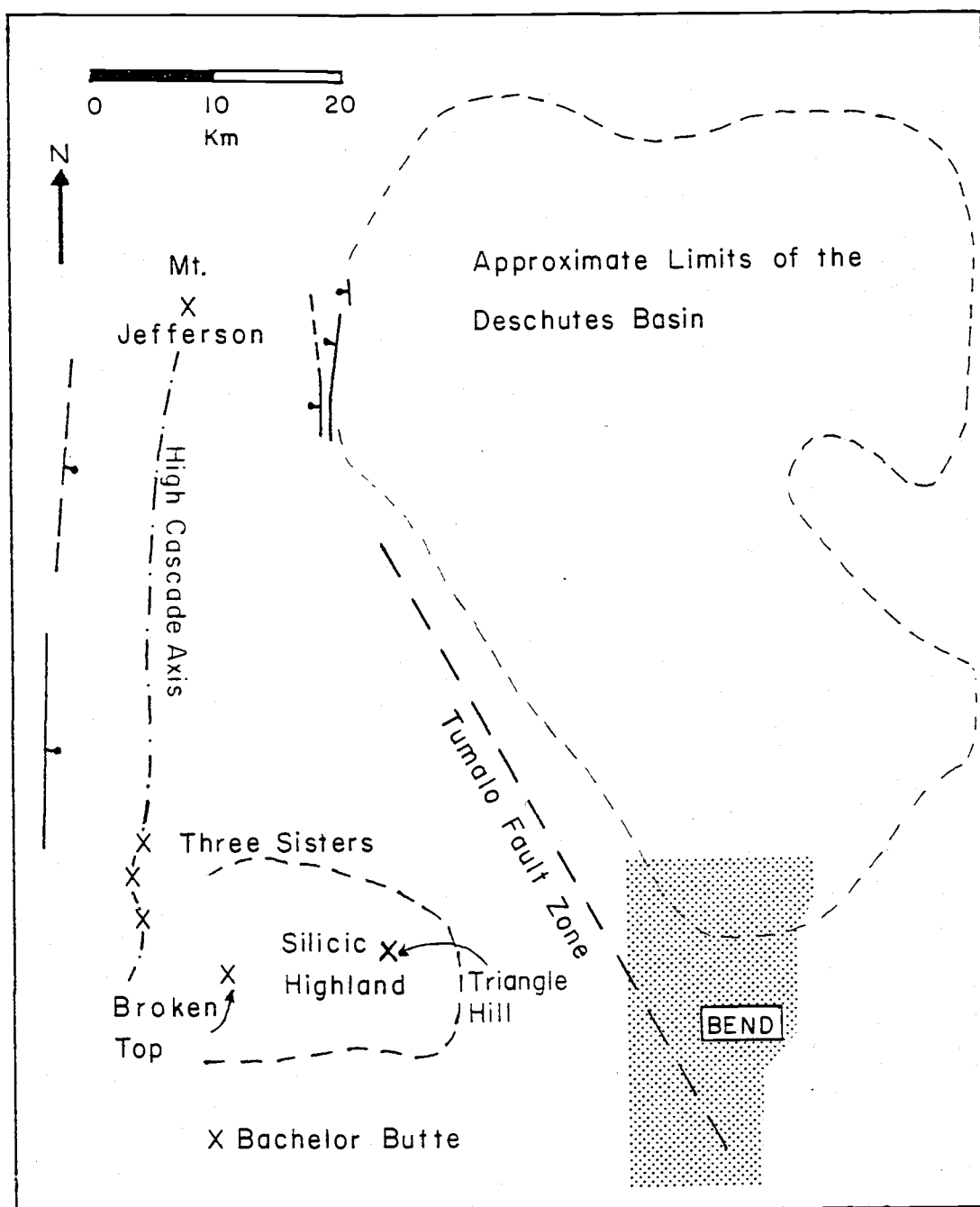


Figure 2: Index map showing general features of the central High Cascades of Oregon.



southwest-to-northeast dispersal pattern for several Deschutes Formation ash-flow tuffs (Cannon, 1984), supports the existence of a large topographic high, coincident with the location of the silicic highland of Taylor (1978), during the late Miocene-early Pliocene. Highland location is shown in figure 2.

The bulk of the present silicic highland was erupted during the early Pleistocene in the form of silicic domes, lava flows, and ash-flow tuffs (Taylor, 1978). The highland has been extensively covered by later Pleistocene mafic lavas and cones, some of which extend east into the study area.

The thesis area contains five different Pleistocene ash-flow tuffs and at least two air-fall lapilli tuffs. From the oldest to youngest, they are the Desert Springs tuff, Bend pumice, Tumalo tuff, Lava Island tuff, Century Drive tuff, and Shevlin Park tuff (Taylor, 1980). An unnamed air-fall lapilli tuff, which occurs stratigraphically above the Tumalo tuff and under the Shevlin Park tuff, is occasionally exposed in the western part of the study area. The Desert Springs, Century Drive, and Shevlin Park tuffs were erupted from vents on the silicic highland (Taylor, 1981). Previous workers (Mimura and MacLeod, 1978; Taylor, 1981; MacLeod et al., 1982; Mimura, in press) have thought the Bend Pumice and Tumalo Tuff were erupted from south of the highland. A detailed stratigraphic column, modified from Peterson et al. (1976) and Taylor (1980) is shown in figure 3.

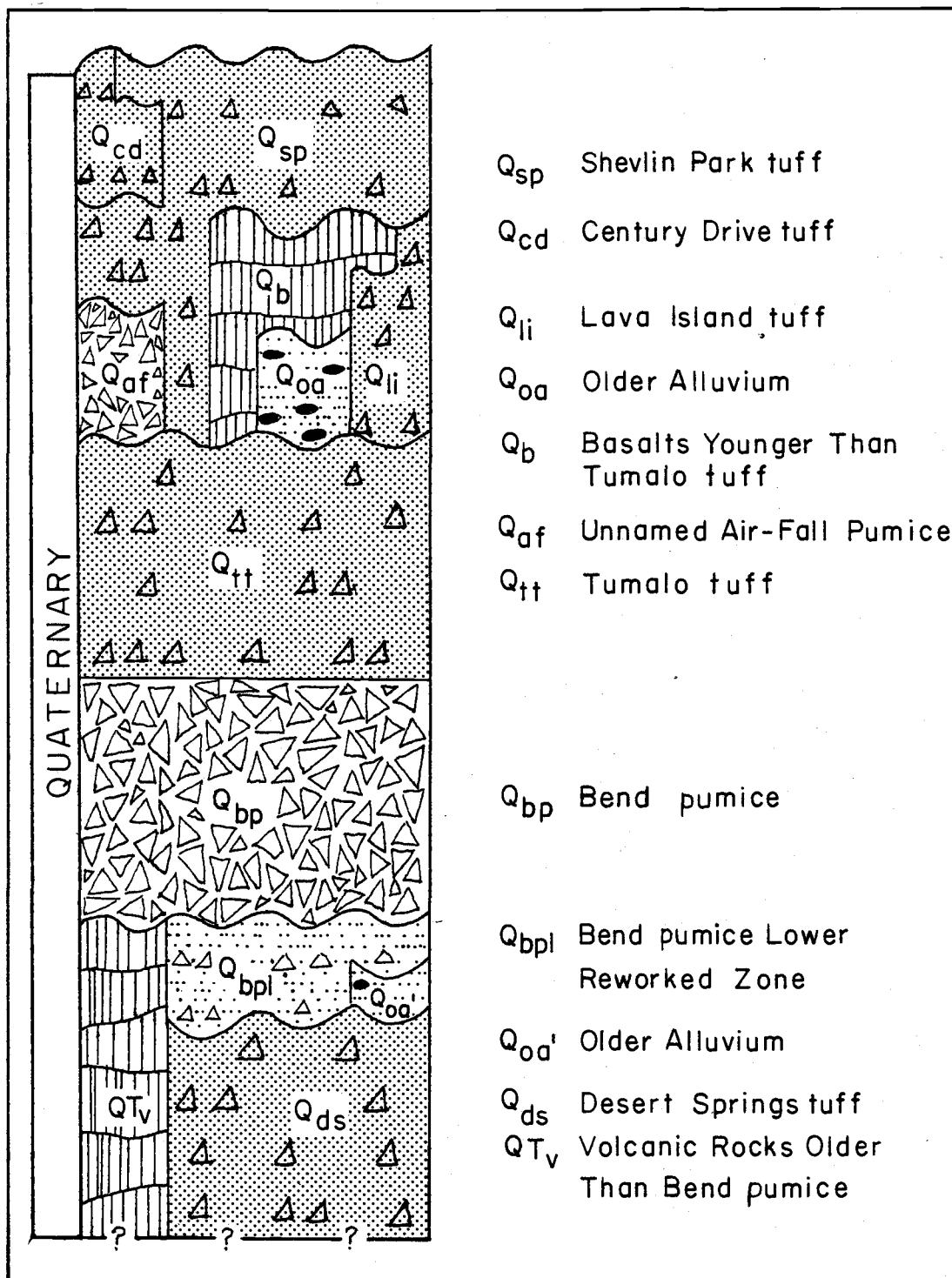


Figure 3: Stratigraphic column of the thesis area, modified from Peterson et al. (1976) and Taylor (1980). See text for detailed explanation.

## 1.4 Magma Mixing and Mixed Pumices

The process of magma mixing in volcanic systems appears to be well accepted in the geologic literature, especially for calc-alkaline compositions. Indeed, "It would be odd if violent eruptions did not result in one magma occasionally entraining another from an adjacent part of the same system" (McBirney, 1980). It is the origin of the contrasting magma types and the significance of mixed pumices that is controversial.

Some researchers attribute magma mixing to the interaction of two independent mafic and silicic systems (eg: Fountain, 1979; Eichelberger, 1975, 1981; Gerlach and Grove, 1982; Yoder, 1973). Others find evidence for zoned magma chambers, in which chemically distinct layers have evolved from a common homogeneous parent and have been mixed during an eruption (eg: Blake, 1981; Smith, 1979; McBirney, 1980).

By definition (Anderson, 1976), magma mixing results in the production of a homogeneous magma. Thus, most mixing arguments are limited to disequilibrium mineral assemblages. Mixed pumices, which contain glasses of at least two different compositions, "...are not evidence of magma mixing, only co-eruption of magma." (Anderson, 1976, after Yoder, 1973) and should not be used as evidence of magma mixing. This opinion of mixed pumices is not universally accepted. Smith (1979), Sparks et al. (1977), MacDonald and Katsura (1965), and Guest (1968), feel that mixed pumices represent the incomplete mixing between two contrasting magma types and that the mixing occurred in

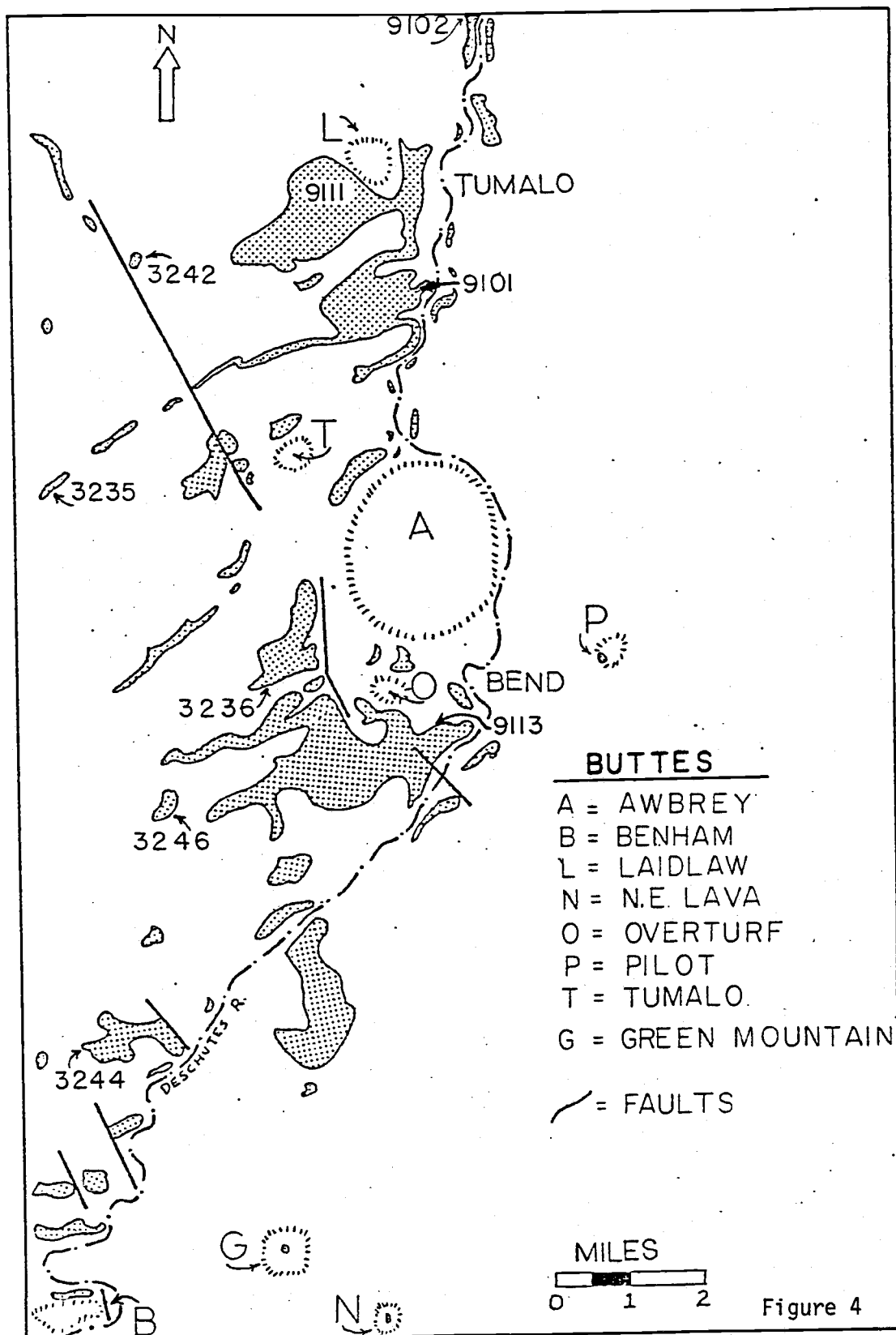
the magma chamber. They feel that mixed pumices should be used as evidence of magma mixing. Mixed pumices are certainly common features of calc-alkaline volcanism, especially in small-volume eruptions of less than  $10 \text{ km}^3$  of magma (Smith, 1979; Sparks et al., 1977). Such small-volume magma systems will tend to form more pronounced temperature and compositional gradients than larger systems, given the same length of residence time (Smith, 1979). During an eruption, mixing of magmas from different zones within a small-volume magma chamber will be inevitable (Blake, 1981; Spera, 1983). Complex "plumbing" systems are also a feature of small, noncaldera forming magma systems, which can allow mixing of magmas from multiple distinct sources (Smith, 1979).

An inherent assumption in this study is that mixed pumices containing two distinct glasses preserved the incomplete mixing of two different magma types at some time during an eruption. The term "mixed pumice", however, shall not imply a particular origin for the contrasting magma types.

### 1.5: Research Methods

The distribution of Bend pumice and Tumalo tuff was mapped at a scale of 1:24,000. A simplified geologic map of the Bend pumice and Tumalo tuff, including sample location sites, is shown in figure 4. Bulk samples of approximately 1.5 kg were collected at two-foot intervals from four vertical sections of Bend pumice (Sites 9101,

Figure 4: Simplified geologic map of the Bend pumice and Tumalo tuff, showing major faults and sample location sites.



9102, 9111, and 9113). Bulk samples were also collected from 5 other Bend pumice exposures, where stratigraphic relationships with the Tumalo tuff were observable. Using a series of standard sieves from -6 phi (64 mm) to 1 phi (0.5 mm), at 1 phi intervals, the bulk samples were manually sifted to avoid excessive abrasion of pumice particles and to determine grain-size weight percentages. Bulk samples of Tumalo tuff were similarly sifted.

Representative pumice lapilli from vertical sections in the Bend pumice, unaltered pumice cores and mixed pumices from the Tumalo tuff, and pumices from unknown units were coarsely ground in a small ceramic mortar. Phenocrysts were removed from the crushed sample magnetically and by removing the sample fraction greater than 0.125 mm through sieving. The resulting powder contained greater than 99 percent glass when viewed under a 60X binocular microscope. When at least 3 g of powder had been processed, the sample was homogenized and split. At least 0.5 g were reserved for instrumental neutron activation analysis (I.N.A.A.) and 2 or more g were reserved for major element oxide analysis.

Nonpumice samples were crushed in a standard jaw crusher and ground to a coarse powder in a rotary plate mill. At least 10 g were then pulverized to a less-than-0.125 mm powder in a Pitchford tungsten-carbide ball mill. The sample was homogenized and 0.5 g powder aliquants were reserved for I.N.A.A.

$\text{SiO}_2$ ,  $\text{TiO}_2$ ,  $\text{Al}_2\text{O}_3$ ,  $\text{FeO}$ ,  $\text{CaO}$ , and  $\text{K}_2\text{O}$  were obtained first after the sample powders dehydrated at 450 °C for 1 hr. Two g of rock powder were then blended with 10 g of an anhydrous lithium metaborate

flux, fused at 1050 °C in a graphite crucible, and molded into a glass button. The base of each button was then ground flat and analyzed by x-ray fluorescence (XRF) equipment utilizing a Cr generating tube coupled to an Ar gas-flow proportional counter. Analyses for  $K_2O$ ,  $SiO_2$ , and  $Al_2O_3$  were made under vacuum. Oxide weight percentages were determined by comparing sample responses to standard response curves for synthesized Cascade rock compositions. Instrumental variation was corrected by means of an internal drift standard and analytical accuracy was determined through analysis of U.S.G.S. rock standards.

Half of each sample button was repulverized. 0.15 g powder aliquants were dissolved in 200 ml of 0.5 N  $HNO_3$ . Abundances of  $Na_2O$  and  $MgO$  were measured using a Perkin-Elmer atomic absorption spectrophotometer (AAS). Standard solutions were run before and after each sample set, to correct for instrumental variation.

I.N.A.A. was done at the Oregon State University Radiation Center, following the procedure outlined in Laul (1979). Samples weighing 0.5 g were irradiated in the rotating rack of the O.S.U. TRIGA Mark 2 reactor for 6 hr at 1 MW (neutron fluence =  $6.5 \times 10^{16}$  neutrons/cm<sup>2</sup>). After a 7-day decay interval, samples were counted for 8,000-10,000 sec on a Ge(Li) gamma-ray detector coupled to a 2,048-channel analyzer system. Na, Ba, La, Nd, Sm, Yb, Lu, and U concentrations were obtained during this counting interval. After one month of further decay, samples were counted on the same system for 20,000 seconds to obtain concentrations of Fe, Co, Cr, Ni, Rb, Sr, Cs, Ce, Eu, Tb, Sc, Hf, Ta, Th, and Zr.



U.S. Geological Survey standards BCR-1 and BHVO-1, along with an in-house rock standard equivalent to BCR-1, were used as standards for this study. Elemental concentrations were obtained through computer and manual reduction of spectral data, using a standard-to-sample peak area comparison method.

Representative plagioclase grains from each unit were finely ground in a ceramic mortar and fused to a glass bead. The bead's index of refraction was then measured, which yielded an average plagioclase composition (Kerr, 1977, p. 311).

Olivine and pyroxene compositions were determined by Dr. E. M. Taylor, using refractive index and 2V measurements of mineral grains oriented on a spindle stage microscope. Additional mineralogical data were obtained through thin section analyses.

Fe-Ti spinels were extracted magnetically from coarsely ground pumices, cleaned in acetone, finely powdered, and analyzed for unit cell dimension with x-ray diffraction equipment. Powder aliquants weighing 0.1 g were then mixed with 1 g of an anhydrous lithium metaborate flux, fused at 1050 °C, and repulverized. 1 g of repulverized button was mechanically blended with 3 g of cellulose and compressed into a wafer. Fe-Ti ratios were obtained through XRF comparison with known standards. Fe-Ti ratios were then compared with unit cell dimensions to determine the extent of post eruptive oxidation of the spinels (Buddington and Lindsley, 1964).

## THE BEND PUMICE

The Bend pumice is divisible into two subunits: a lower reworked zone (LRZ) and an upper air-fall zone (UAZ). Both units were produced from the Bend-Tumalo source volcano and represent tephra from the air-fall phase of plinian eruptions.

## 2.1 Lower Reworked Zone (LRZ)

The LRZ is best exposed north of Tumalo State Park, along Tumalo Market Road (SE 1/4, NW 1/4, Sec 6, T17S, R12E); and in several abandoned pumice quarries southwest of Bend (NE 1/4, SW 1/4, Sec 6, T18S, R12E). Figure 5 shows locations where recognizable LRZ is exposed. The LRZ lies disconformably over plane-bedded alluvial sands and gravels or the Desert Spring ash-flow tuff. Thickness of the LRZ is locally variable and ranges from 1 to 3 m.

The character of the LRZ changes irregularly throughout the study area. It is usually found as a massive deposit of reworked pumice lapilli and ash, disseminated within alluvial sands and gravels. The pumice fragments are hydrated and have undergone varying degrees of collapse, forming a deposit of barely distinguishable lapilli within disseminated sand and gravel (figure 6). The LRZ can grade from a massive deposit to one in which rounded pumice lapilli are confined to discrete lenses and beds within coarsly bedded alluvium. Reworked pumice lapilli within these beds

Figure 5: Generalized geologic map of the Bend pumice and Tumalo tuff showing locations of active and abandoned pumice quarries, and recognisable exposures of Bend pumice lower reworked zone.

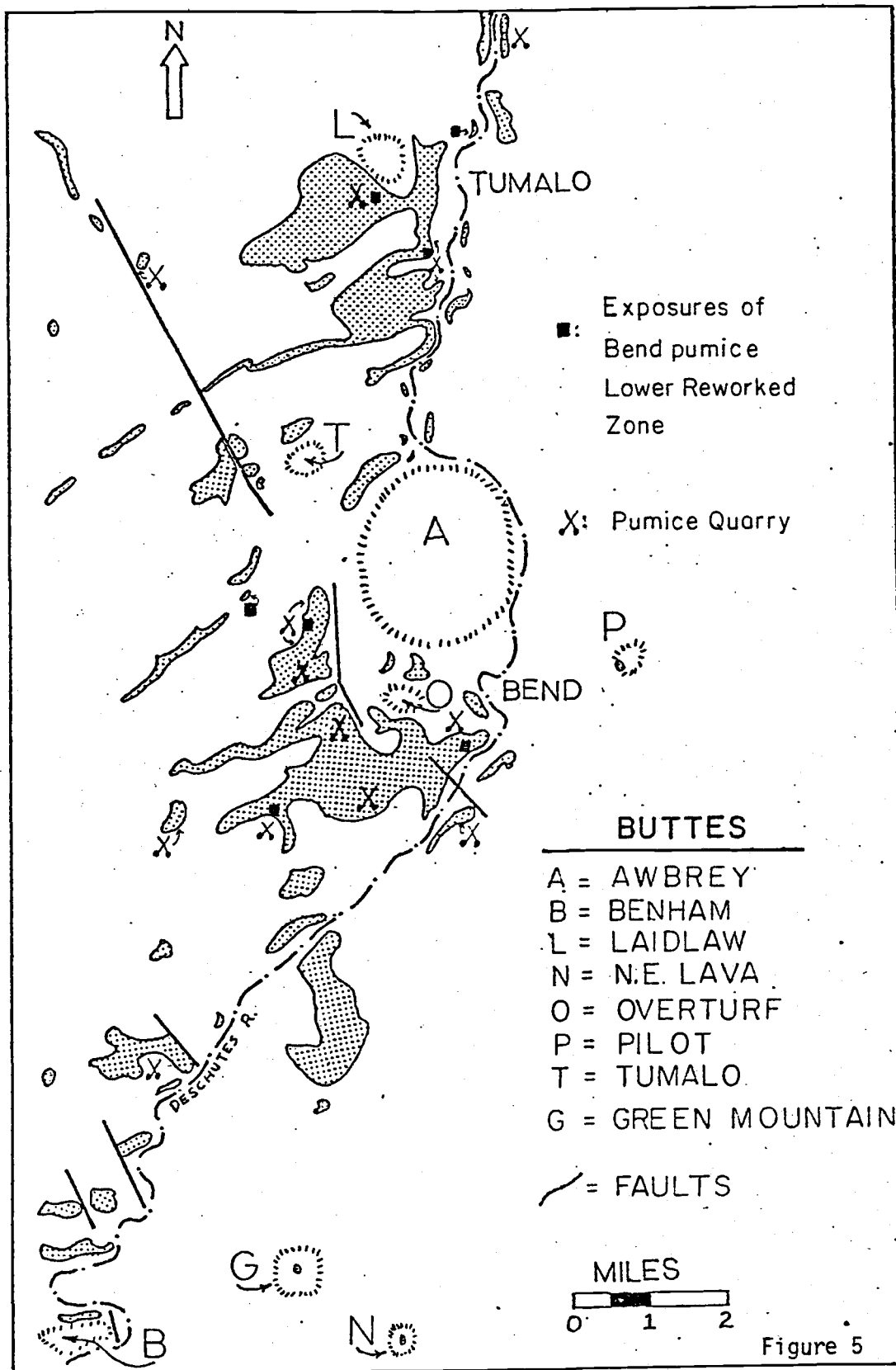




Figure 6: Lower reworked zone of the Bend pumice. Darker fragments are perlitic obsidian.

and lenses are unaltered and are often faintly graded. Occasionally 0.5-meter-thick beds are found within the alluvium, consisting of fresh angular pieces of pumice. Unreworked beds represent pristine air-fall pumice deposits, which were rapidly covered by alluvium.

Carbonized wood and perlitic obsidian fragments are also characteristic of the LRZ. Carbon is scarce and consists of several 1- to 3-cm-long twig and branch fragments at the upper contact of one LRZ exposure. Approximately 1 cm<sup>3</sup> pieces of light gray obsidian are disseminated throughout the LRZ. The obsidian was hydrated after emplacement, forming a fragile perlite. The obsidian probably represents a dome or plug which was fragmented during the opening stages of the Bend-Tumalo eruption.

During the preliminary stages of the eruption, the thin layer of pumice which uniformly mantled the topography was reworked rapidly and concentrated in drainages. The upper contact of the LRZ is irregular and usually distinct with the base of the upper air fall zone. This contact represents a hiatus in the Bend-Tumalo eruption, of sufficient length to permit minor hydration and reworking of the pumice.

## 2.2 Upper Air-Fall Zone (UAZ)

The main unit of the Bend Pumice, the upper air-fall zone (UAZ), is best exposed in numerous pumice quarries throughout the study area. Quarry locations are shown in figure 5. Exposed thickness of

the UAZ, which is rarely complete, ranges from 2 to 13 m. The major components of the UAZ are: pumice lapilli (approx. 70%), volcanic ash (20-25%), volcanic rock fragments (3-5%), and free crystals (<<1%). The Bend pumice is a poorly consolidated vitric air-fall lapilli tuff (Schmid, 1981). A typical section of UAZ Bend pumice is shown in figure 7.

Pumice lapilli from the UAZ of the Bend pumice are found on Awbrey, Laidlaw, Overturf, Pilot, and Tumalo Buttes (figure 4). Bend pumice lapilli are also present on the summit of Green Mountain. A two-meter-thick section of UAZ Bend pumice is also exposed on the northern flank of Benham Butte. Benham Butte is a rhyodacitic dome complex, having a K-Ar age of  $1.75 \pm 0.8$  m.y. (McLeod et al., 1982). The Bend pumice is probably younger than 1.8 m.y. and can be no older than 2.6 m.y.

Drilling logs for water wells in the Bend area show a 1- to 25-m-thick white pumice deposit located near the surface throughout the area (Oregon Dept. of Water Resources, 1982). While water-well logs are generally imprecise in their lithologic descriptions and depths, it is reasonable to assume that this deposit is the UAZ of the Bend pumice. A simplified isopach map from well-log data is shown in figure 8. There is a general west-to-east thinning of the UAZ, although it is not possible to determine if the trend is from the south or north of west.

There are no known Bend pumice exposures which could represent either coarse proximal or fine distal deposits. With such limited exposure, only a minimum estimate of volume can thus be derived for



Figure 7: Typical section of the Bend pumice upper air-fall zone. Note the freshness of the deposit and occasional larger lithic fragments.



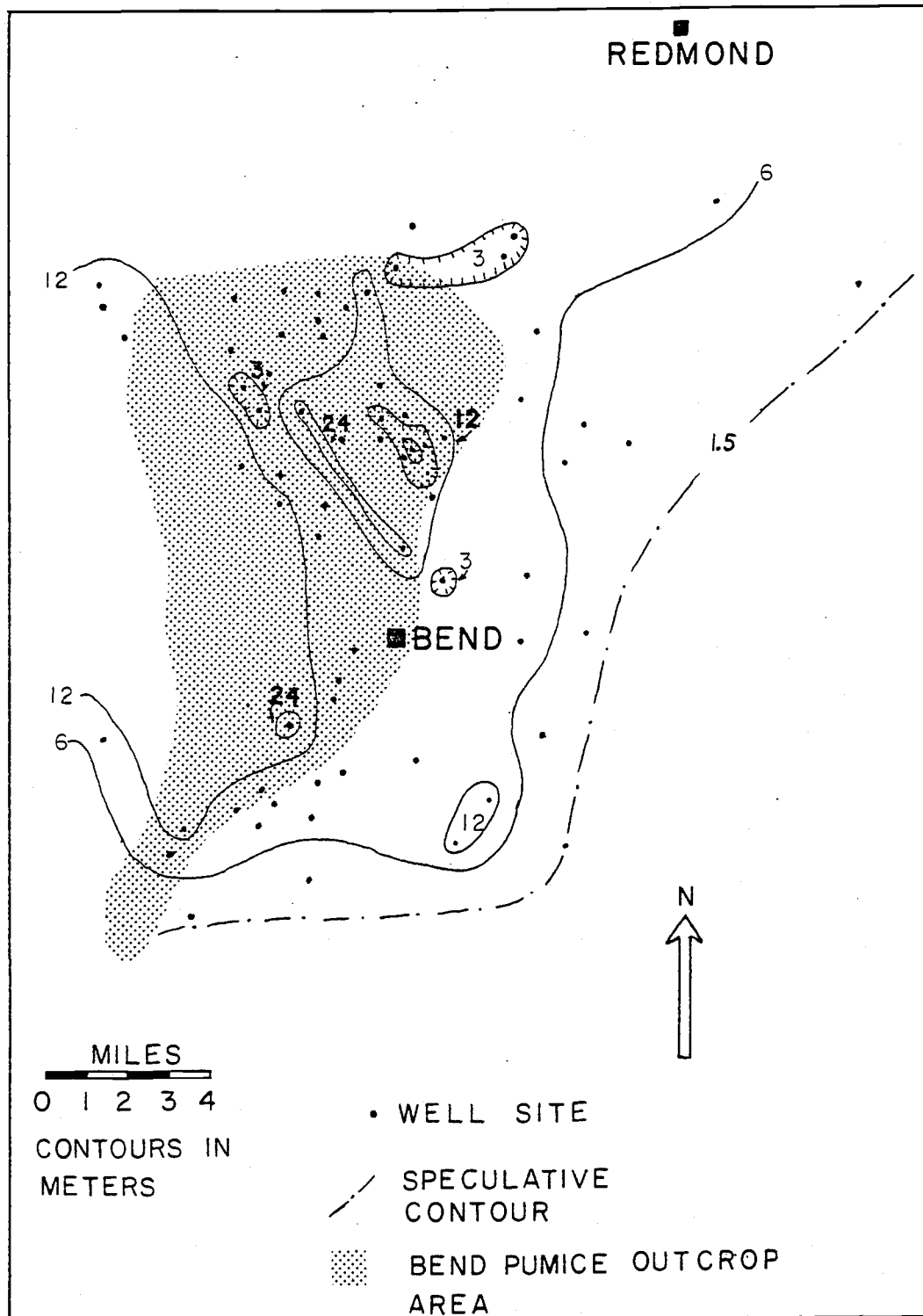


Figure 8: Bend pumice subsurface isopach map from water well-log data.

the Bend pumice. The Bend pumice is presently exposed over 150 km<sup>2</sup>. Assuming an average thickness of 5 m throughout the area, 0.8 km<sup>3</sup> of Bend pumice tephra is preserved. The density of rhyolitic magma at 800 °C is 2.3 g/cm<sup>3</sup> (Murase and McBirney, 1973). In-situ Bend pumice deposits have a bulk density of about 0.3 g/cm<sup>3</sup> (E.M. Taylor, pers. comm.), a low value which reflects a porosity of approximately 50%. The silicic magma that produced the Bend pumice must have vesiculated 87% to produce these density contrasts. Therefore, a minimum of 0.4 km<sup>3</sup> of silicic magma must have been erupted to produce the Bend pumice. The eruption undoubtedly involved a much greater volume of magma; distal ash deposits, which have not been recognized for the Bend pumice, could comprise more than 75% of the total bulk of the eruption (Lidstrom, 1971).

### 2.3 Grain Size Analysis

Fisher (1964), Sparks (1976), Walker (1971,1981), and Frogatt (1982) provide excellent reviews on the variation of statistical grain-size parameters in pyroclastic deposits. Owing to limited vertical and lateral exposure, statistical parameters will provide the most useful information on source direction and character of the eruption that produced the Bend pumice. The parameters Md (median grain diameter) and Ss (simple sorting) are derived from cumulative frequency curves and refer to the grain size at 50 weight % and 1/2(84 wt% - 16 wt%), respectively.

Using the terminology of Walker (1971), the Bend pumice is a monocomponent deposit, having less than 5% lithic fragments and free crystals. With the absence of intradeposit ash beds or readily discernable grading, the Bend pumice should be similar to most other Plinian air-fall deposits and have a fairly homogeneous grain-size distribution throughout each vertical section (Walker, 1971). Analysis of four vertical sections of Bend pumice (sites 9101, 9102, 9111, and 9113 in figure 4) shows a large variation in Md and Ss with height in the Bend pumice section. These data are shown in table 1, with their simplified cumulative frequency curves plotted in figures 9 and 10. The Bend pumice shows a general trend of increasing Md up section to a level 1-2 meters below the top of the unit. At that level the Md decreases roughly 25% over a distance of 0.5 meters. Up to this level the slopes of the cumulative frequency curves remain reasonably constant. From the fine zone to the top of the unit Md again increases. Within this interval the cumulative frequency curves trend across earlier curves, reflecting a lower degree of sorting at the top of the Bend pumice. This trend of regularly shifting Md and Ss is repeated throughout the area, at the same relative height in each section.

There is no evidence in the form of intraplinean ash-beds of discernable unconformities within the Bend pumice to indicate that there was a hiatus in the eruption of the UAZ. It is possible that the reverse grading and Md shifts in the Bend pumice UAZ are due to variations in wind direction during the eruption. However, for wind shifts to occur simultaneously throughout a 150 km<sup>2</sup> area and for

Sample	D(m)	GRAIN SIZE (phi)								
		<u>-6</u>	<u>-5</u>	<u>-4</u>	<u>-3</u>	<u>-2</u>	<u>-1</u>	<u>0</u>	<u>&gt;0</u>	<u>-Md</u>
9101H	0	0	11	6	17	18	21	13	14	2.1
9101G	0.9	0	3	5	13	21	22	18	18	1.6
9101D	1.5	0	3	12	25	24	21	10	6	2.6
9101C	2.1	0	1	7	19	24	26	13	10	2.0
9101B	2.7	0	1	3	14	20	26	11	25	1.5
9101A	3.3	0	4	5	14	20	26	16	14	1.7
9102A	0	0	3	10	17	18	19	17	16	1.9
9102D	0.9	0	1	6	16	19	31	14	14	1.7
9102G	1.5	0	2	6	14	23	28	25	11	1.8
9102H	2.1	0	2	9	20	23	25	11	10	2.2
9111C	0	0	12	10	19	18	19	11	12	2.4
9111D	0.9	0	3	13	20	19	20	12	14	2.2
9111G	1.5	0	1	4	13	20	31	20	12	1.6
9111H	2.1	0	4	13	24	23	22	9	5	2.6
9111J	2.7	0	6	16	19	21	21	9	7	2.5
9111K	3.3	0	2	7	19	22	28	14	9	2.0
9111L	3.9	0	2	5	13	21	26	21	12	1.7
9111M	4.5	0	1	5	13	19	27	21	14	1.5
9111N	5.1	0	0	8	15	20	26	19	13	1.5
9111A	5.7	0	1	3	12	21	29	23	12	1.4
9111B	LRZ	0	0	1	8	21	32	23	12	-
9113A	0	0	11	18	17	18	17	10	8	2.7
9113B	0.6	0	11	11	16	16	18	12	15	2.2
9113C	1.7	0	4	9	17	19	22	15	7	1.9
9113G	2.4	5	4	10	22	22	19	10	4	2.6
9113J	3.6	0	7	8	16	26	20	10	11	2.3
9113L	4.8	0	3	5	16	25	25	15	11	2.0

Table 1: Bend pumice grain-size weight percentages. D= distance below Bend pumice - Tumalo tuff contact. Columns refer to bulk weight percentages. Md= median diameter in phi units.

## 9102 DESCHUTES RIVER RANCH

## 9101 TUMALO STATE PARK

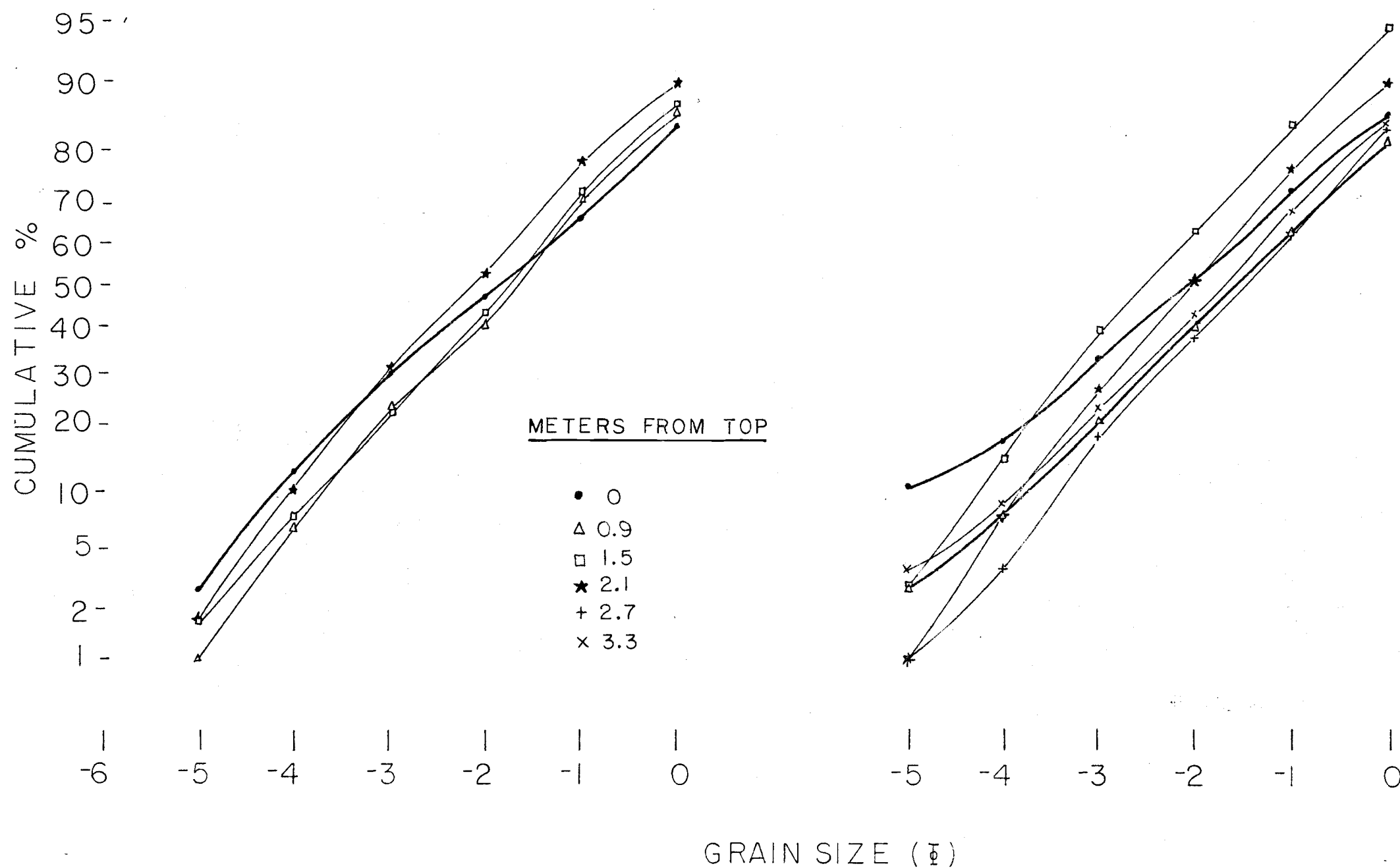


Figure 9: Cumulative frequency curves for Bend pumice sections located at Deschutes River Ranch (9102), and Tumalo State Park (9101).

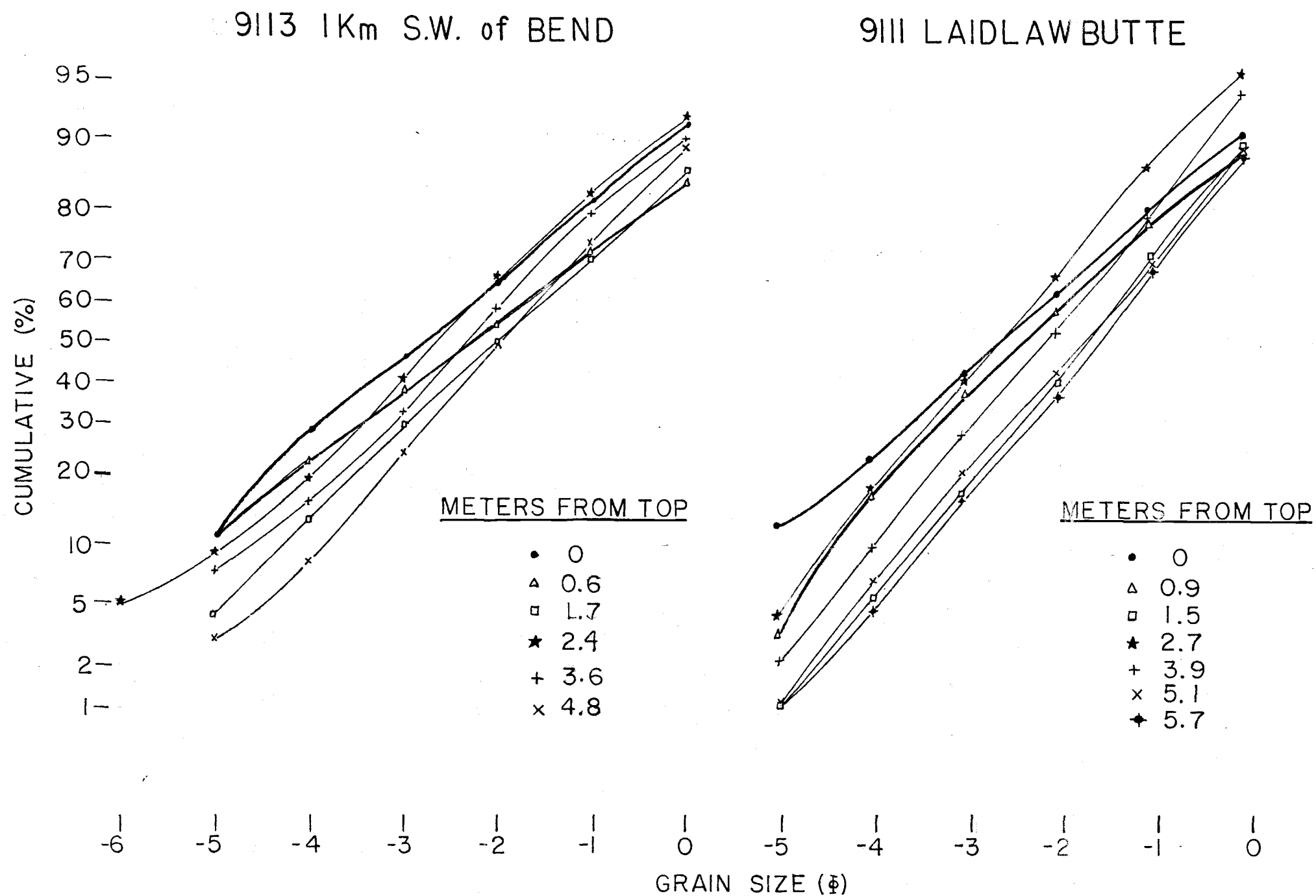


Figure 10: Cumulative frequency curves for Bend pumice sections located at Laidlaw Butte (9111) and west of Bend, Oregon (9113).

those shifts to cause only reverse grading (Wilson et al., 1980) and decreased sorting seems very unlikely.

Lapilli from the Bend pumice are less than 10 cm in diameter, and therefore were not transported ballistically away from the vent (Wilson, 1976); lapilli-sized pumice is entrained in the eruption column and carried upward by convection. Varying magmatic gas pressure, which will primarily control ejection velocities of large (>10 cm) pumice clasts, will have thus had little effect on grading of Bend pumice at sites far removed from the source vent. Wilson et al. (1980) have shown that an increase in the radius of a vent will increase the convection and height of an eruption column. Larger pumices will then be carried to a higher altitude and transported farther downwind from the vent. They conclude that reverse grading is primarily caused by progressive widening of the vent and has little to do with variations in the gas content of the magma.

Probably during eruption of the Bend pumice, vent radius gradually increased, producing the observed reverse grading up to 1-2 meters from the top of the UAZ. Vent radius then apparently decreased for a short time perhaps due to a temporary obstruction, which resulted in the formation of the finer-sized pumice zone. Once the vent was cleared of the possible obstruction, the Md continued to increase. Deposits of this final interval were enriched in coarse lapilli, which resulted in poorer sorting. At the top of the UAZ, the Md is roughly equal to the Md prior to the formation of the fine zone. This Md appears to be a function of the critical vent radius, in excess of which the walls of the vent were unstable. A final

collapse of the vent walls might have increased the vent radius to a point where upward flow could no longer support the mass of the eruption column. The plinian column may have then collapsed and formed the Tumalo ash flow.

The Bend pumice has no normally graded top, which should be present if the eruption had gradually ceased and pumices in the eruption column remnants had settled through gravity sorting. Emplacement of the Tumalo Tuff did not result in discernable erosion into the Bend pumice. Deposition of the UAZ was apparently terminated by the emplacement of the Tumalo ash-flow tuff.

Samples used to determine the location of the Bend pumice source vent must come from the same stratigraphic interval to avoid variations due to reverse grading. The interval from 10 to 50 cm below the contact with the Tumalo tuff was chosen because it is easily recognised and is relatively well exposed. An isomedian map (figure 11) for that interval shows that the source vent of the Bend pumice was located to the west of Bend. The prevailing wind was blowing slightly to the southeast, giving an elongated dispersal pattern to the Bend pumice.

The distance to the source vent is more difficult to estimate. Median diameters for air-fall deposits will not always be a simple exponential function of distance from the vent, due to the addition of ballistically transported pumice near the vent. Assuming a limiting  $M_d$  of 0.002 mm and an exponential trend of  $M_d$  (Fisher, 1964), the Bend pumice must have extended at least 80 km further to the southeast. However, only a 10-km-long segment of Bend pumice is



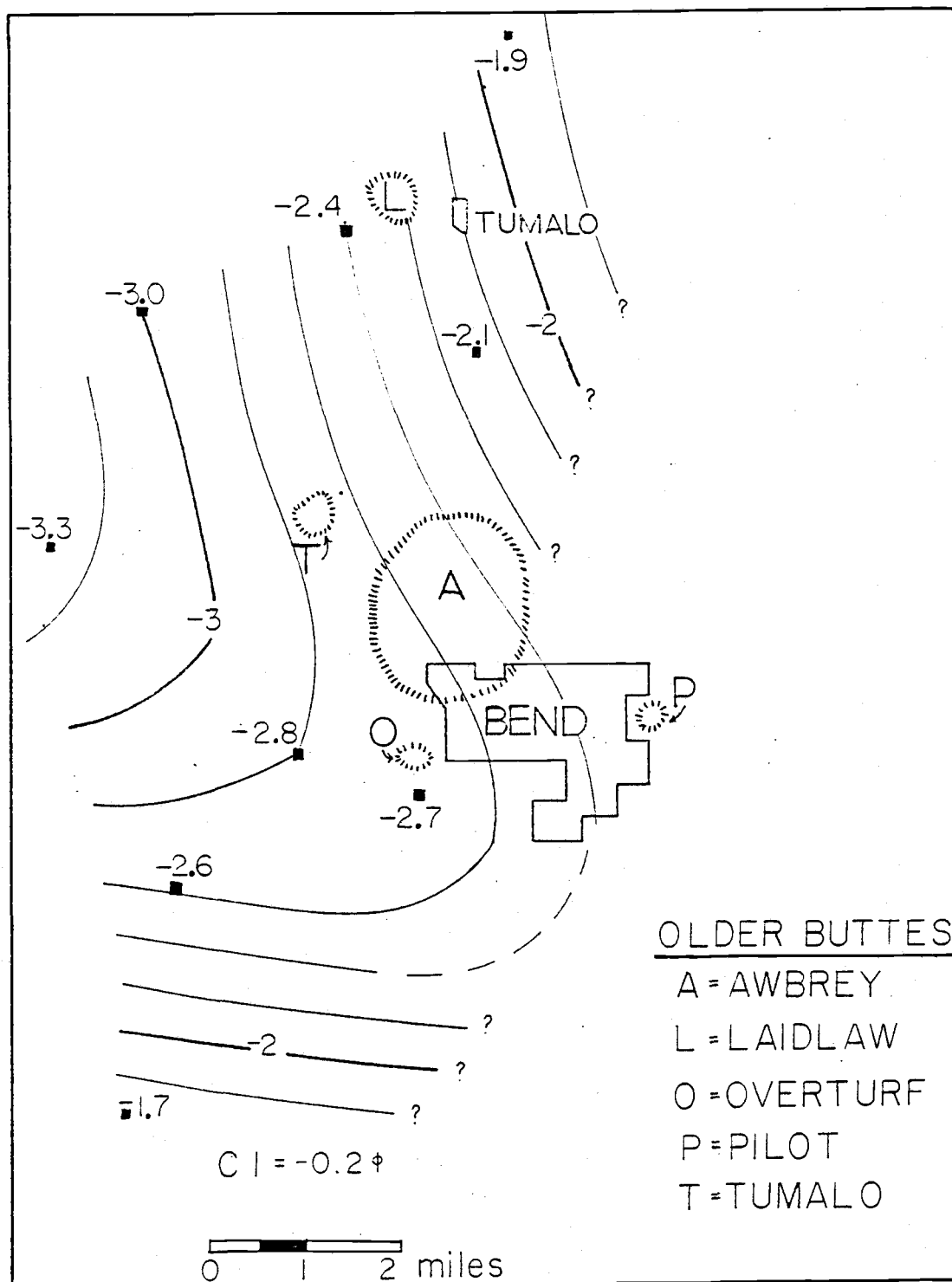


Figure 11: Isomedian map for the Bend pumice, using median grain-size diameters from the upper 10 to 50 cm of the deposit.

preserved from which to extrapolate, so this extent must be viewed as an approximation. Three possible source locations are considered on longitudes approximately equal to Triangle Hill, Broken Top, and the High Cascade axis (figure 2). These locations give respective distances of 5, 10, and 15 km from the assumed vent to the coarsest exposure of Bend pumice, along an axis defined by the elongate dispersal pattern shown in figure 11. Md versus assumed distances are plotted in figure 12, along with exponential best fit curves having coefficients of determination equal to 0.969. Data presented by Fisher (1964) and Walker (1971) show that near-vent Md's greater than 3.2 cm are rare and that there is a high frequency of 0.4 to 1.6 cm Md's approximately 10 km away from known vents. Figure 12 shows that these data best apply to the Bend pumice if a source was 5 to 10 km west of the coarsest exposure, i.e. on the silicic highland between Broken Top and Triangle Hill. While a source on the High Cascade axis cannot be entirely eliminated, it would necessitate a proximal deposit with a Md of at least 5.6 cm, a value which is rarely reported in the literature. A source location greater than 20 km from the coarsest exposure does not appear reasonable for the Bend pumice.

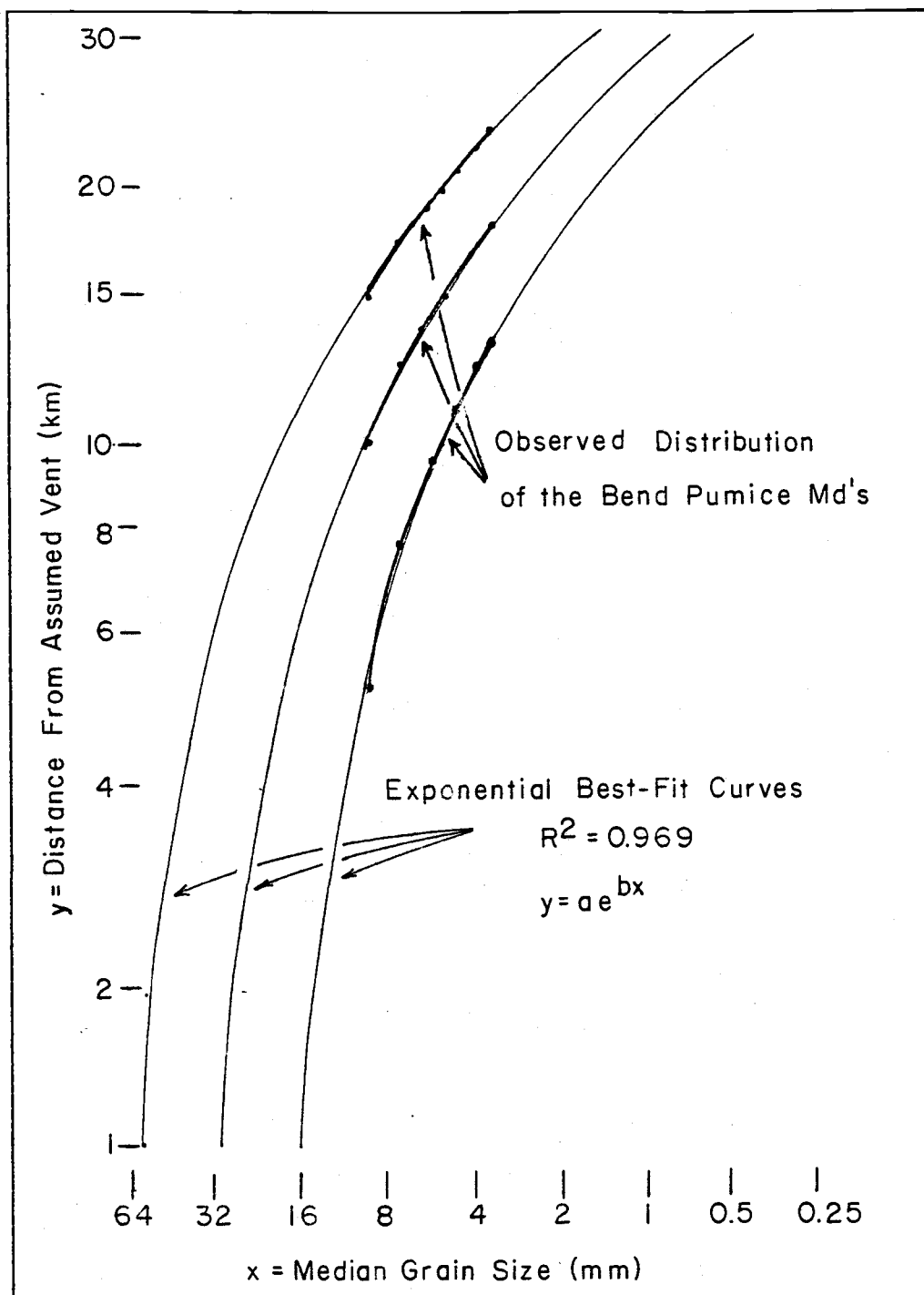


Figure 12: Median grain size versus distance from 3 possible vent locations, with exponential best-fit curves.

## THE TUMALO TUFF

The Tumalo tuff is a rhyodacitic ash-flow tuff, produced in the culminating stages of the Bend-Tumalo eruption through column collapse. The one flow unit present in the Tumalo tuff is divisible into three distinct members: a rarely observed, basal, coarse-pumice layer 1(P) (Wilson and Walker, 1982), a basal, coarse-pumice-depleted layer 2a, and the main nonsorted layer 2b (Sparks et al., 1973). Proximal Tumalo tuff deposits contain mixed pumice blocks and lapilli, which preserve the mixing between two distinct magmas. The Tumalo tuff has undergone post-emplacement vapor-phase alteration, and is variably welded.

### 3.1 Layer 1(P)

The nongenetic term "layer 1(P)" was defined by Wilson and Walker (1982) to describe coarse pumice-enriched deposits found at the base of some ash-flow tuffs. These deposits are in distinct contact with the overlying ash-flow tuff, yet were deposited from the same ash flow. Layer 1(P) deposits are depleted in fine material, laterally discontinuous, and in places clast supported.

Exposures of layer 1(P) in the Tumalo tuff are restricted to one 20-meter-long outcrop 8 km southwest of Bend, which is shown in figure 13. The 1(P) deposit is in sharp contact with both the

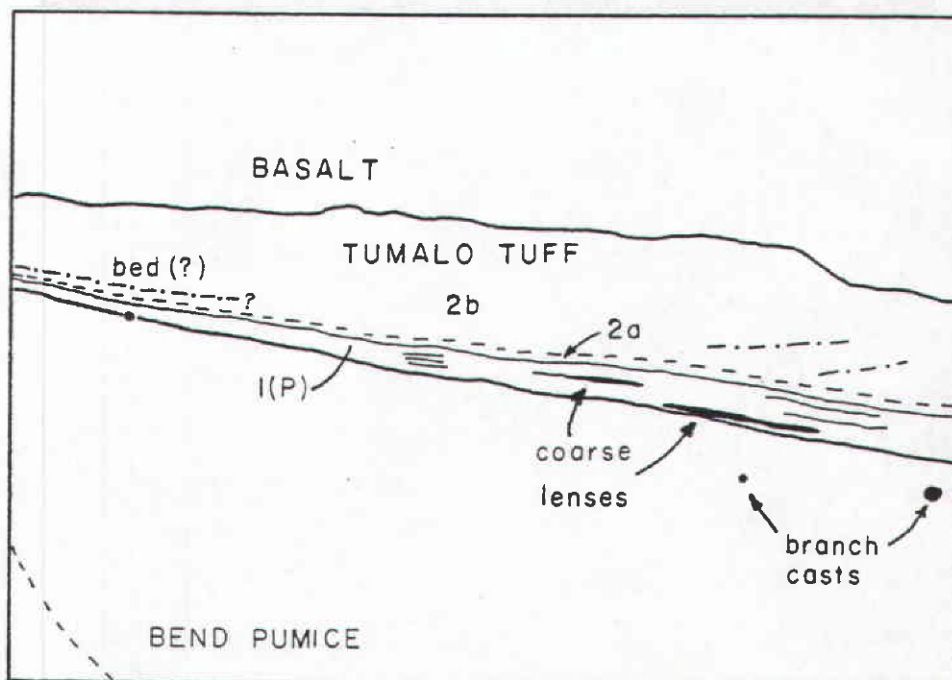


Figure 13: Proximal features of the Tumalo tuff, including layer 1(P). Tumalo tuff thickness is approximately 1.5 m.

underlying Bend pumice, and the overlying layer 2a of the Tumalo tuff. Layer 1(P) does not extend more than 20 m west or east of this exposure. The Tumalo tuff layer 1(P) in figure 13 also shows the faint stratification and irregular thickness which are characteristic of 1(P) deposits. Note the apparent bedding in the lower part of the Tumalo tuff layer 2b, which may have been produced when the main part of the Tumalo ash flow traveled over irregularities on the upper surface of the 1(P) deposit. Discrete lenses of well rounded pumice in clast support are also found in the Tumalo tuff layer 1(P).

It is suggested by Wilson and Walker (1982) that 1(P) deposits are formed when a large pocket of air is ingested into the leading edge of an ash flow. Rapid heating and expansion of the trapped air will cause forward portions of the flow to jet ahead, elutriating fine ash from the jet and emplacing a coarse-pumice enriched 1(P) deposit. It is likely that this process produced the Tumalo tuff layer 1(P), although a genetic model can only be inferred from this exposure.

### 3.2 Basal Layer 2a

As with most other ash-flow tuffs, the Tumalo tuff has a coarse-pumice depleted, basal 2a layer. It is developed best in more distal eastern exposures where it can range up to 1.5 m thick, although it is present in all exposures. Layer 2a is characterized by a 0.1- to 1-m-thick bed of white-to-tan ash and pumice, which

grades upward into the coarser, main unsorted 2b layer.

Cumulative frequency curves for two Tumalo tuff sections are shown in figure 14. Data for these curves are given in table 2. The basal 2a layers for both Tumalo tuff sections have lower median pumice diameters and are better sorted than their corresponding 2b layers. The curves for each 2a-2b pair converge toward finer grain sizes, which indicates that the 2a layer was formed through coarse pumice depletion, not fine pumice enrichment (Sparks, 1976).

Coarse pumice is reversly graded in layer 2a by two processes, both of which operate simultaneously in ash flows. Pumice lapilli are generally less dense than the surrounding ash-flow matrix. When this density contrast is maintained, the buoyant force on a pumice increases as the cube of its diameter. Thus, larger pumices are more susceptible to grading than smaller ones. Sparks (1976, after Bagnold, 1954) has also shown that at the basal boundary of an ash flow, grain dispersive forces which operate normal to flow direction are sufficient to buoy larger pumices upward into the main (2b) part of the flow. Dispersive force rapidly diminishes upward from the flow base, as flow-induced shear will also decrease upward from the flow base. This results in smaller pumices being buoyed into the main layer as the distance above the base of the flow increases, producing a reverse graded deposit in layer 2a. The transition from 2a to 2b marks the point in which grain-dispersive force is effectively zero; the reverse grading which is observed in layer 2b of some ash-flow tuffs is only the product of density sorting.

Localized irregularities occur in the basal 2a layer of the

<u>SAMPLE</u>	GRAIN SIZE (PHI) %									
	<u>-6</u>	<u>-5</u>	<u>-4</u>	<u>-3</u>	<u>-2</u>	<u>-1</u>	<u>0</u>	<u>1</u>	<u>1.5</u>	<u>&gt;1.5</u>
9102 2a	0	0	1	2	4	7	9	12	5	61
9102 2b	0	3	3	5	6	8	8	9	4	54
9113 2a	0	1	2	4	8	13	10	9	5	50
9113 2b	3	1	8	9	8	10	9	9	4	39

Table 2: Tumalo tuff grain-size weight percentages. Sample 9102 is from a 5-meter-thick section of Tumalo tuff exposed 0.1 km west of Deschutes River Ranch. Site 9113 is from a 7-meter-thick section of Tumalo tuff exposed in an abandoned pumice quarry located 1 km southwest of Bend, Oregon. Cumulative frequency curves for these data are given in figure 14.



$\Delta$  = 9102 (2b)  
 $\blacktriangle$  = 9102 (2a)  
 $\circ$  = 9113 (2b)  
 $\bullet$  = 9113 (2a)

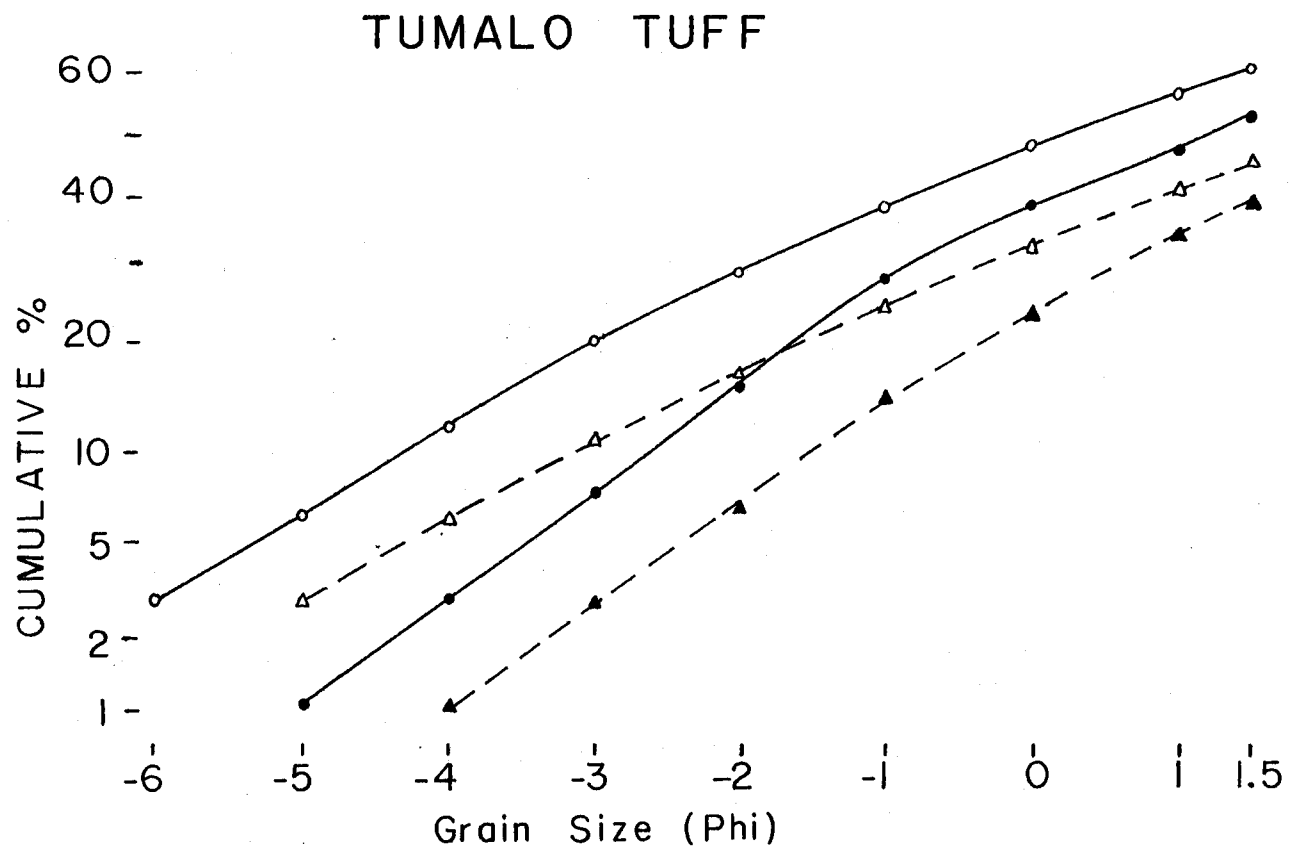


Figure 14: Cumulative frequency curves for two Tumalo tuff sections, contrasting layers 2a and 2b.

Tumalo tuff. Laterally discontinuous layers of coarse pumice, with some blocks up to 20 cm in diameter, are shown in figure 15. These coarse layers are best explained as the result of localized turbulence or fluidization in the ash flow, which reduced the density of the ash-flow matrix. Coarse pumice was then able to sink into the basal layer. Note that the coarse pumices do not rest on the Bend pumice; there was still sufficient grain-dispersive force to maintain the pumices in the ash flow. These coarse layers could easily be confused with the coarse-pumice enriched zones which occur at the top of some ash-flow tuffs

The presence of multiple reverse graded layers within the basal 2a layer of the Tumalo tuff is shown in figures 16 and 17. Similar features are found in distal exposures of other large pyroclastic flow units, although their origin has not been determined (Sheridan, 1979). Note the gradational nature of the contacts between each reverse graded unit in figure 16, and in figure 17, how the layers merge and coarsen over a declivity in the paleotopography. These features seem to preclude formation of the reverse graded layers through separate events, such as multiple surges in front of the ash flow or individual flow lobes. It is more likely that several discrete velocity gradients existed on top of each other in the base of the Tumalo tuff ash flow in its distal reaches; one continuous velocity profile is indicated in proximal deposits, where there is only one reverse graded unit in layer 2a. A diagram of these possible flow conditions is shown in figure 18. Once coarse pumice had dropped into the basal layers of the flow, it would then

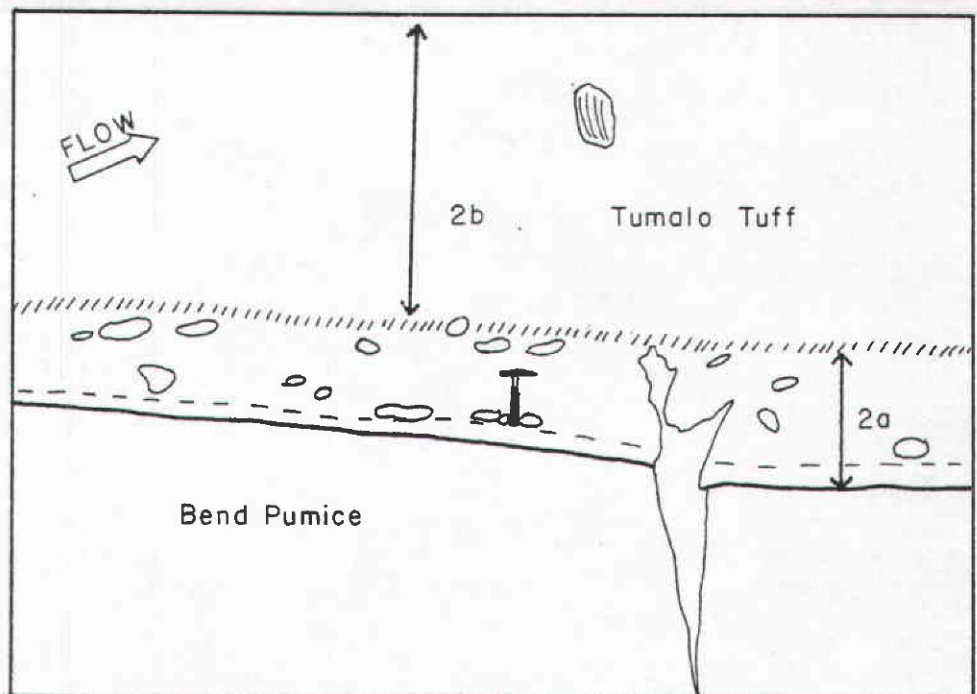


Figure 15: Layer of coarse pumice within the basal layer 2a of the Tumalo tuff. 1 km southwest of Bend, Oregon. Hammer is 30 cm long.

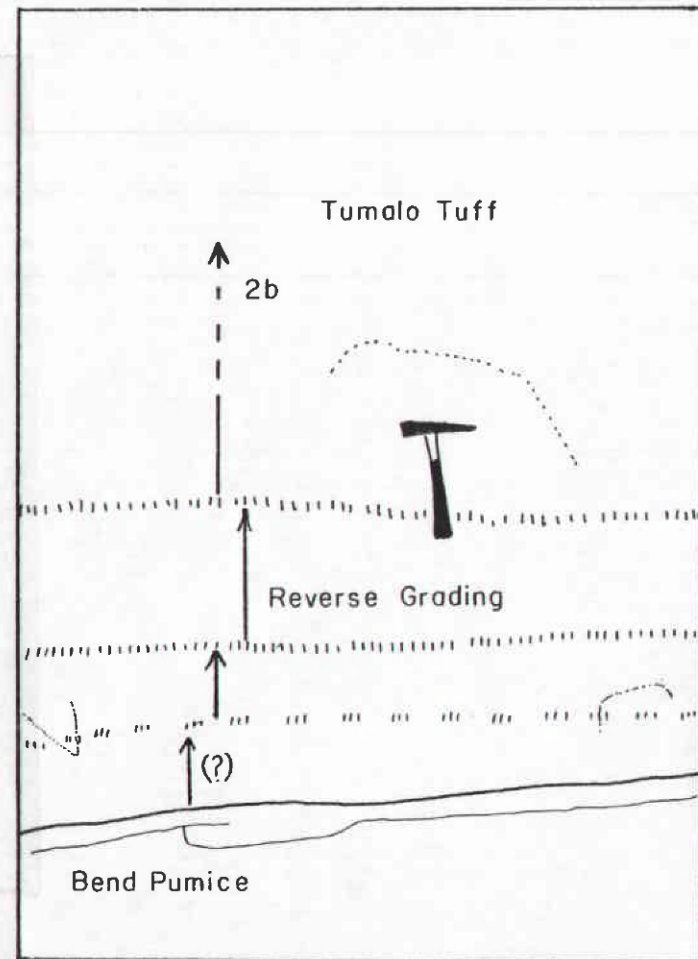


Figure 16: Multiple reverse-graded units within layer 2a of the Tumalo tuff, exposed in an abandoned pumice quarry southeast of Tumalo State Park. Hammer is 30 cm long.

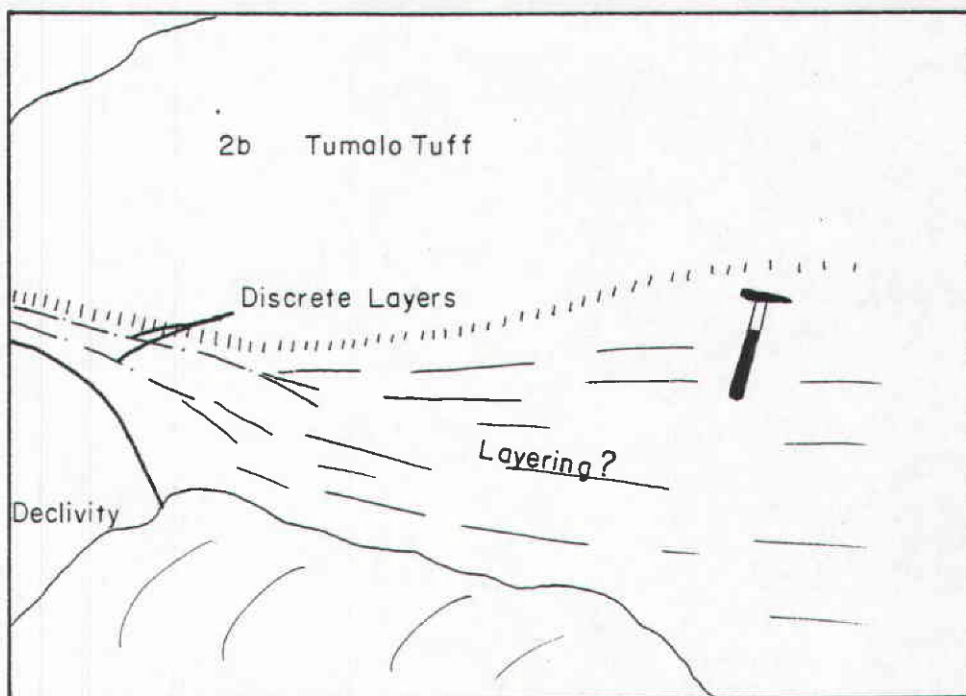


Figure 17: Coarsening and thickening in layer 2a of the Tumalo tuff in response to a declivity in the Bend pumice, approximately 20 m south from figure 16.

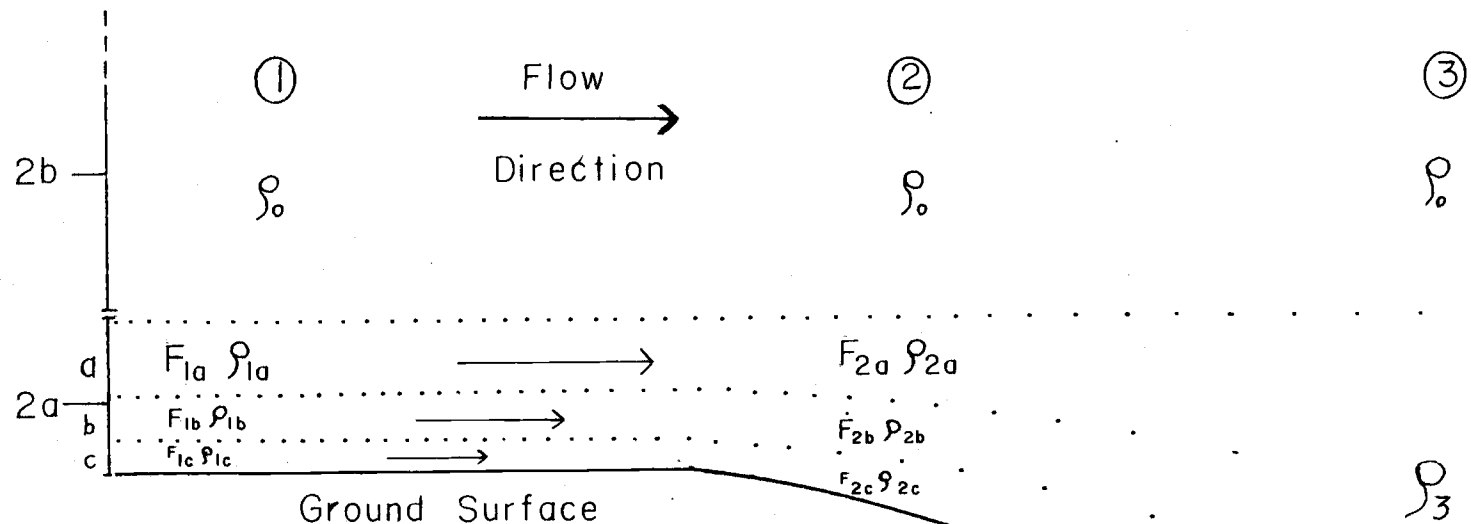


Figure 18: Diagram of possible flow conditions in the base of the distal Tumalo ash flow.  $F$  = Grain dispersive force,  $\rho$  = ash-flow density,  $F_c \& \rho_c > F_b \& \rho_b > F_a \& \rho_a$ . Point 1 = Undisturbed distal flow conditions, with 3 discrete flow zones in layer 2a.  $\rho_0 > \rho_{1(a,b,c)}$ . Point 2 = Ash flow passes over declivity; expansion of layer 2a decreases  $F_{(a,b,c)}$  &  $\rho_{(a,b,c)}$  to  $\rho_0 < \rho_{2(a,b,c)}$ . Pumice from layer 2b settles into layer 2a, and is graded in  $2a_{(a,b,c)}$ . Point 3 = Turbulence induced by flow over declivity results in  $\rho_0 \ll \rho_3$ ; turbulence also homogenizes  $2a_{(a,b,c)}$ , resulting in no grain dispersive force.

segregate within each velocity layer through grain dispersive force, producing several reverse graded units. Figure 17 shows that as the Tumalo tuff ash flow passed over a declivity in the Bend pumice surface, coarse pumice from the main part of the flow dropped into the basal layer, coarsening and thickening it. Turbulence induced by passage of the ash flow over the declivity also disrupted the velocity profiles which existed at the base of the flow. Away from the declivity, separate velocity profiles were maintained, as shown by the lateral continuity of the reverse graded layers in figure 17.

### 3.3 Main Nonsorted Layer 2b

Layer 2a of the Tumalo tuff grades upward into the main nonsorted layer 2b. The main components from layer 2b are: 1) pumice lapilli (10-30%); 2) basaltic to andesitic rock fragments (5-15%); 3) volcanic ash (60-80%); and 4) free crystals (approximately 1%). The Tumalo tuff is thus a vitric ash-flow tuff. Layer 2b is the product of one episode of flow, with the greater-than-ash-sized components not discernably graded in vertical section. The lack of grading reflects the high particle concentration within the ash flow, which inhibited vertical movement of pumice and rock fragments (Sparks, 1976).

The bulk of the Tumalo tuff is contained in the 2b main nonsorted layer. Layer 2b has a preserved thickness which ranges for 1 to 25 m, although a complete section is not exposed. To derive a



minimum volume estimate for the Tumalo Tuff, it is assumed that a minimum thickness of 10 m is present throughout a  $150 \text{ km}^2$  area;  $1.5 \text{ km}^3$  of tephra is thus preserved. Nonwelded Tumalo tuff has a density of  $0.4 \text{ g/cm}^3$  (E.M. Taylor, personal comm.). Although some of the Tumalo tuff is welded, assuming the entire unit to be nonwelded will produce the lowest minimum volume estimate. Under these assumptions, a minimum of  $0.8 \text{ km}^3$  of rhyodacitic magma was erupted to produce the Tumalo tuff.

In more proximal western exposures up to 2% of the pumice in the Tumalo tuff is of mixed compositions (figure 19). These pumice blocks, which can range up to 50 cm in diameter, preserve the incomplete mixing between the rhyodacitic magma which comprises the bulk of the Tumalo tuff, and a dacitic magma. Owing to their large size and higher density, mixed pumice blocks tend to concentrate at the base of layer 2b, although they do not form a discrete layer.

Invasion of dacitic magma into the erupting reservoir could have increased the gas content of the reservoir as injection of a dacitic magma would abruptly increase vesiculation in the cooler rhyodacite. This may have abruptly increased the eruption rate and velocity, which could have widened the vent beyond its critical diameter and initiated column collapse. Because the Tumalo tuff was emplaced on top of the Bend pumice before the air fall was completely deposited, it is extremely likely that the Tumalo tuff was produced through collapse of the same eruption column that produced the Bend pumice. The effect of invasion of dacitic magma into the erupting reservoir is speculative and column collapse is not dependent on a



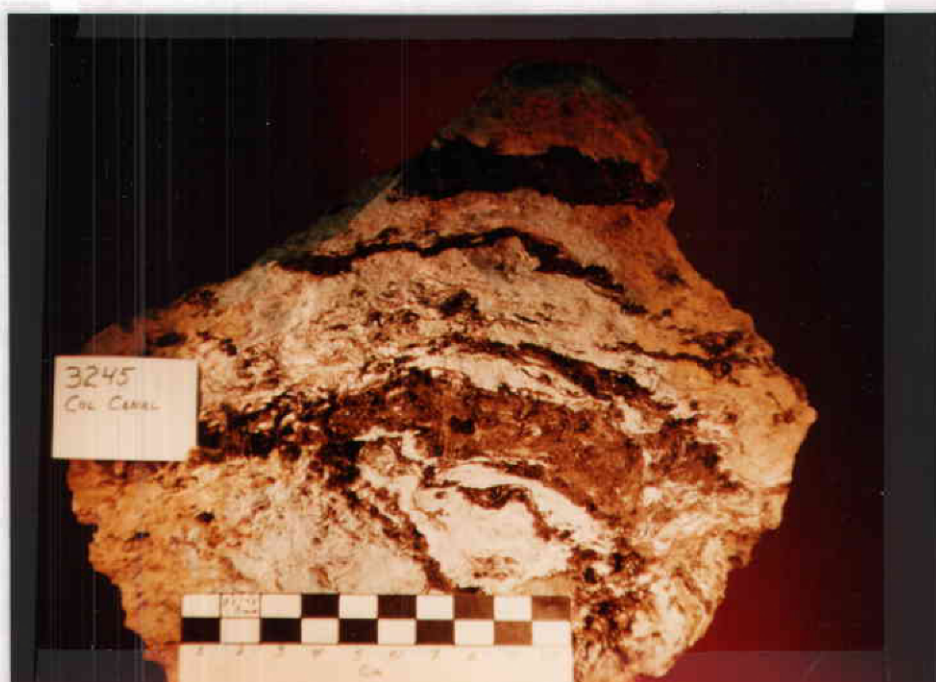


Figure 19: Mixed pumice from the Tumalo tuff.

mixing event (Sparks and Wilson, 1976).

The top of layer 2b is not readily discernable in exposed sections. Tumalo tuff in roadcuts along Highway 20 near Laidlaw Butte show a slight coarse pumice enrichment near the top of a 20-meter-thick section, which may represent the top of layer 2b. Apparent coarse pumice enrichment may be due to erosion of the ash-flow matrix at the top of the outcrop. A coarse pumice-enriched zone, which has an uncertain location in the Tumalo Tuff section, is exposed near Tyler Road, in NW 1/4, SE 1/4, Sec 11, T 17 S, R 11 E.

Other observable internal features of layer 2b are limited in occurrence to one exposure located 8 km southwest of Bend (site 3246, figure 4). Tumalo tuff at this exposure contains a 1-m-thick zone enriched in rock fragment, which is located approximately 2 meters above the base of layer 2a. The origin of this rock fragment enriched zone is uncertain, though it may represent a more proximal deposit containing a greater percentage of source-derived rock fragments. The rock fragment enriched zone does not continue more than 100 m east of this outcrop, and is not exposed to the west.

In the absence of measurable changes in thickness or observable channel-boundary features, it is difficult to demonstrate that the Tumalo ash flow was significantly channeled by the underlying paleotopography. Previous workers have attributed the Tumalo tuff to a vent located southwest of Bend, based in part on pumice imbrication in the basal layer of the Tumalo tuff (Mimura and MacLeod, 1978; Mimura, in press). While pumice imbrication is occasionally developed in the basal layer of the Tumalo tuff, it is not a

continuously observed feature. Also, imbrication is controlled by flow direction and ground surface configuration (Sparks, 1976), and may not reflect a source direction if the ash flow traveled over a highly dissected terrain. It has been demonstrated in this work that the Tumalo tuff was emplaced immediately following deposition of the Bend pumice; the Bend pumice and Tumalo tuff were probably products of the same eruption. Chemical and mineralogical similarities, which will be discussed in later chapters, further supports production of these units from the same eruption. It has also been shown that the Bend pumice was erupted west of Bend, from a vent coincident with the location of the silicic highland. If the Tumalo tuff was erupted today from the silicic highland, it would flow east off of the highland until it was channeled by the northeast-trending drainage system near Bend and would show southwest-oriented pumice imbrication. An analogous drainage system must have existed at the time of the B-T eruption to account for the southwest-oriented pumice imbrication in the Tumalo tuff.

### 3.4 Post Emplacement Effects

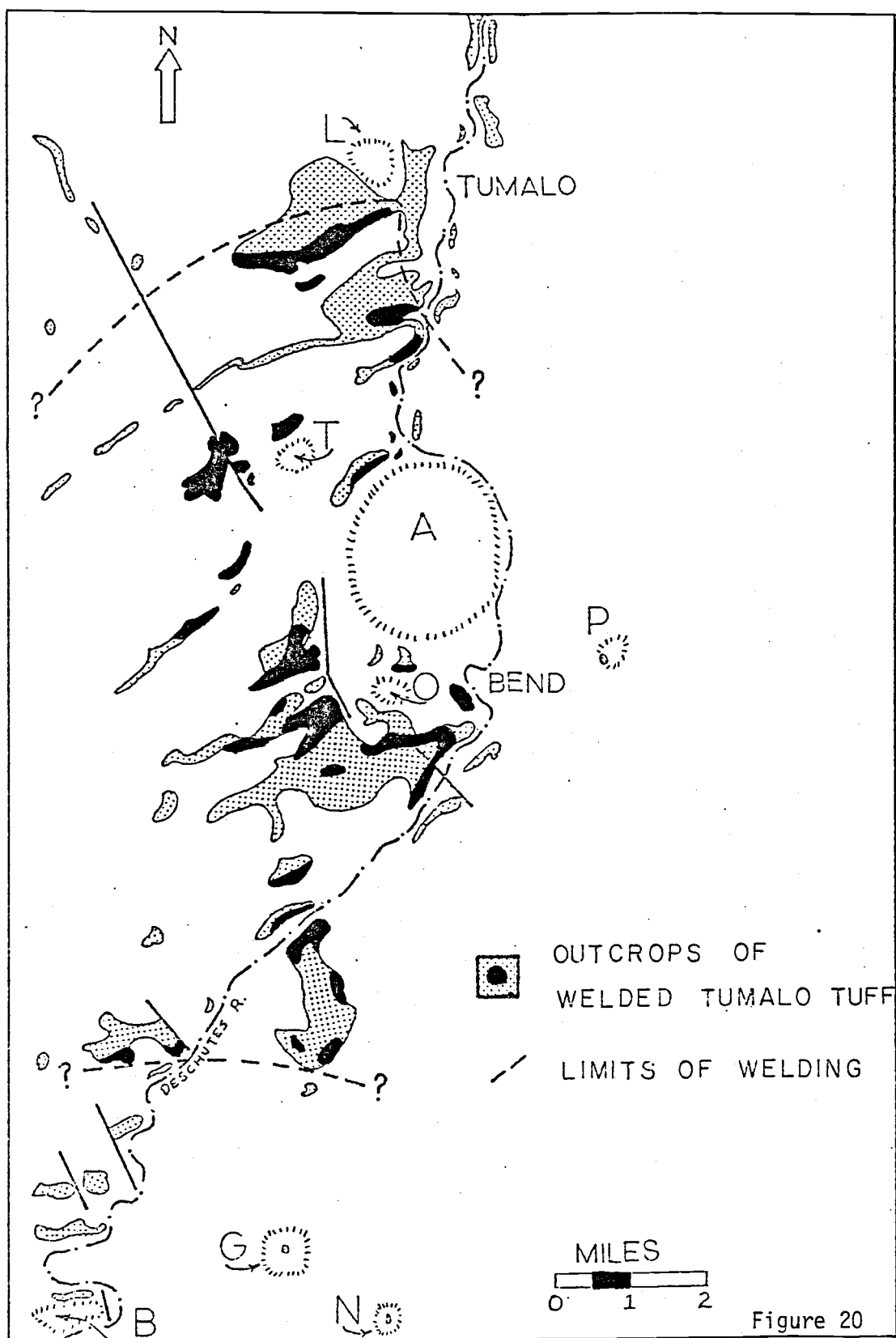
Post emplacement effects in the Tumalo tuff consist of welding, vapor-phase alteration, induction of remnant magnetism, and erosion. The Tumalo tuff has undergone little alteration due to weathering. Pumice and glass shards, where not affected by vapor-phase

alteration, are fresh.

Approximately 40% of all Tumalo tuff exposures are welded to some degree, with welded outcrop thickness ranging up to 10 m. The distribution of welded Tumalo tuff is shown in figure 20. The original thickness of the welded zone is uncertain, as the top of all welded exposures is an erosional surface. The degree of welding is laterally variable and can range from incipient to nonwelded in less than 10 m. Most of the welding in the Tumalo tuff is incipient, with no glass shard deformation and little pumice collapse. Welding can at times include moderate shard deformation, associated with more extensive pumice collapse.

Welding in the Tumalo tuff does not appear to be a function of thickness. The degree of welding in a 10-meter-thick section does not appreciably increase downward. Incipient welding is developed 2 to 3 m above the base of the Tumalo tuff in numerous 7-to-10-meter-thick outcrops. If it is assumed that welding was developed about one third of the way up-section (Smith, 1960) and that thickness primarily controlled the development of welding, then all Tumalo tuff exposures of thicknesses greater than 10 meters should show indications of welding. There are several 20-meter-thick exposures of Tumalo tuff which show no indication of welding. These thick, nonwelded exposures indicate that emplacement temperature, and not the thickness of the unit, governed the degree of welding in the Tumalo tuff. Ash-flow tuff derived from cooler portions of the eruption column, or flow zones which had ingested greater amounts of cool air while traveling away from the vent (Smith and Bailey, 1966),

Figure 20: Simplified geologic map of the Bend pumice and Tumalo tuff, showing the distribution of welded Tumalo tuff. Letter symbols as in figure 4.



became less welded.

With the exception of the basal layer, all of the Tumalo tuff has undergone vapor-phase alteration after emplacement. The effects of vapor-phase alteration are minimal, and consist of oxidation and hydration of iron oxide within the glass, giving the Tumalo tuff a characteristic pink-to-tan color. Some large pumice lapilli show concentric zones of alteration, grading from fresh gray glass in the cores to orange-brown glass in the rims. In thin section the altered glass appears to be coated with limonite and has not been devitrified.

Vapor-phase alteration did not result in discernable mobility of the major elements, nor were additional phases crystallized in the glass during alteration. Alteration first appears just below the 2a-2b contact, suggesting that the lack of alteration in the basal layer is due to a vapor/gas flux which was too low to produce alteration, or that the base of the Tumalo tuff was emplaced below the vapor-blocking temperature of the glass.

Welded Tumalo tuff is normally polarized and is overlain by at least six different normally polarized High Cascade mafic lava flows. Another overlying basalt flow northwest of Awbrey Butte is magnetically reversed, based on three different samples obtained near the massive base of the flow. To account for this overlying reversed flow, the Tumalo tuff must have been emplaced prior to the end of the Jaramillo Normal Event 0.89 m.y.b.p.; the Jaramillo Event is the last known North American period of normal polarity followed by a magnetic reversal.

## MINERALOGY

As there are no observed mineralogical differences between the Bend pumice and Tumalo tuff, their mineralogy will be discussed as if they were one unit and their pumice will be jointly referred to as B-T pumice. In the B-T rhyodacitic pumices, crystals make up less than 1% of the total pumice weight. For dacitic bands in the Tumalo tuff mixed pumices, crystals comprise 1 to 2% of the pumice weight. Phenocrysts are dominantly euhedral and unaltered unless otherwise stated.

Average compositions of plagioclase crystals were determined through index of refraction measurements on fused powders following the procedure outlined in chapter 1. Pyroxene and olivine compositions were determined through mineral 2V and index of refraction measurements obtained on a spindle stage microscope by Dr. E. M. Taylor.

#### 4.1 Plagioclase

Sodic andesine having an average composition of  $An_{32}$  is the only feldspar in the B-T pumice. The andesine can range in length up to 5 mm although 1 mm is average. Polysynthetic twinning is rarely observed in thin sections of B-T andesine. The lack of visible twin planes may be due to cleavage of the andesine during magma



vesiculation, leaving only thin (010) cleavage fragments. Poorly developed normal zoning is observed in approximately 25% of thin sectioned B-T andesines, with the outer one-quarter of the crystal being slightly more sodic than the cores.

Calcic andesine having an average composition of  $An_{48}$  is the distinguishing and most abundant feldspar in the mixed pumice dacite, although two distinct plagioclase populations are occasionally present. Calcic andesines in the dacite have better developed polysynthetic twinning than B-T andesines and occasionally show both albite and Carlsbad twinning. The dacitic calcic andesines also have a slight normal zoning and show no evidence of resorption.

The dacitic pumice occasionally contains a second plagioclase population, which consists of variably resorbed, unzoned and untwinned plagioclases containing up to 75% brown glass inclusions. Owing to their lack of polysynthetic twinning and abundant glass inclusions, no compositions could be determined. The dacitic sieved-textured plagioclases could represent relict plagioclases from a prior mixing event, or earlier crystallized calcic plagioclase in disequilibrium with a more evolved dacitic melt.

#### 4.2 Pyroxenes

Clinopyroxene is restricted in occurrence to minor amounts of small anhedral-to-subhedral phenocrysts in the mixed pumice dacite. The clinopyroxene is augite and does not appear to have reacted with

the dacitic melt. Lack of obvious reaction rims argues against the augites being xenocrysts; their anhedral to subhedral morphology is unusual in the predominately euhedral dacitic mineral assemblage.

Orthopyroxene is the dominant ferromagnesian mineral in the B-T pumice. The orthopyroxene is ferrohypersthene  $Fs_{58}$  and occurs as both acicular and short, complexly terminated prisms. Both forms can range in length up to 2 mm and do not appear to be zoned in thin section. In the central High Cascades, high-iron ferrohypersthene are rarely found (E. M. Taylor, pers. comm.) and reflect the highly evolved nature of the B-T rhyodacitic magma.

The mixed pumice dacite contains hypersthene  $Fs_{38}$  in relatively minor amounts. The dacitic hypersthene also occur as short prismatic and acicular phenocrysts which range in length up to 2 mm. They do not appear to be zoned in thin section and show no evidence of resorption or reaction with the dacitic melt.

#### 4.3 Amphibole

B-T pumice contains relatively minor amounts (Plg>Opx>Hb>Mgt>Ap>Zr) of black, acicular cleavage fragments of hornblende, which can range in length up to 2 mm. While the composition of the hornblende is unknown,  $n_g = 1.676$  and  $ZAC = 14^\circ$ ; it is apparently not oxyhornblende. Of greater significance is the lack of an olivine or pyroxene core, or a pyroxene/opacitic reaction rim around the hornblende. In silicic melts, hornblende is generally

formed through the reaction and replacement of earlier crystallized olivine or pyroxene (Gill, 1981). B-T hornblende shows none of the features associated with subliquidus formation and appears to have crystallized directly from the rhyodacitic melt.

Hornblende is the major ferromagnesian mineral in the mixed pumice dacite (Plg>Hb>Opx>Ol>Mgt>Ap>Ilm>Cpx>Zr). The dacitic hornblendes have  $n_x = 1.700$  and are olive-green in thin section. The acicular hornblendes have a maximum extinction angle of  $5^\circ$ , although they do not appear to be oxyhornblendes. They are acicular in form and range in length up to 2 cm, although an average length is 0.2 cm. The dacitic hornblendes do not show evidence of an olivine or pyroxene core, or a reaction rim and appear to be a liquidus phase. Their large size and lack of abundant glass inclusions precludes their formation through quench crystallization or devitrification (Anderson, 1980).

It is unusual to find apparently liquidus-phase hornblende in equilibrium with dacitic and rhyodacitic melts, if the pertinent literature is accepted. Experimental data for hornblendes in high-silica systems are extremely limited (Helz, 1982); thus, only generalizations can be made about their occurrence in the Bend pumice and Tumalo tuff. Extrapolating from reported data on andesitic systems, it appears that at least 2% water must have been present in these melts for hornblende crystallization (Anderson, 1980). The melts probably began crystallization under at least 5 kbars pressure (Jakeš and White, 1972). While it must be emphasized that these conditions are only crude approximations for the B-T and dacitic

hornblendes, they do indicate that the magmas did not crystallize under anhydrous, near surface (< 1 km) conditions.

#### 4.4 Olivine

Olivine is restricted in occurrence to the mixed pumice dacite, where it occurs as euhedral phenocrysts up to 0.5 mm long. The olivines are moderately iron-enriched and have a composition of  $Fa_{44}$ . Olivine occurs in approximately the same abundance as hypersthene in the dacitic pumice. The olivines do not appear to be resorbed, nor do they have pyroxene reaction rims.

#### 4.5 Oxides and Accessory Phases

Titanomaghemite occurs in both B-T and dacitic pumices as octahedral and dodecahedral microphenocrysts and as inclusions in nearly every orthopyroxene phenocryst. Two analyses of B-T titanomaghemite, as obtained through the XRF/XRD procedure outlined in chapter 1, are shown in figure 21. The spinels have a pre-eruption composition of  $Usp_{42}$  and have undergone significant post-eruption oxidation to titanomaghemite.

Minor but significant amounts of ilmenite occur in the mixed pumice dacite. The hexagonal plates of ilmenite can range up to 0.5 mm in width and show no visible signs of alteration or corrosion.

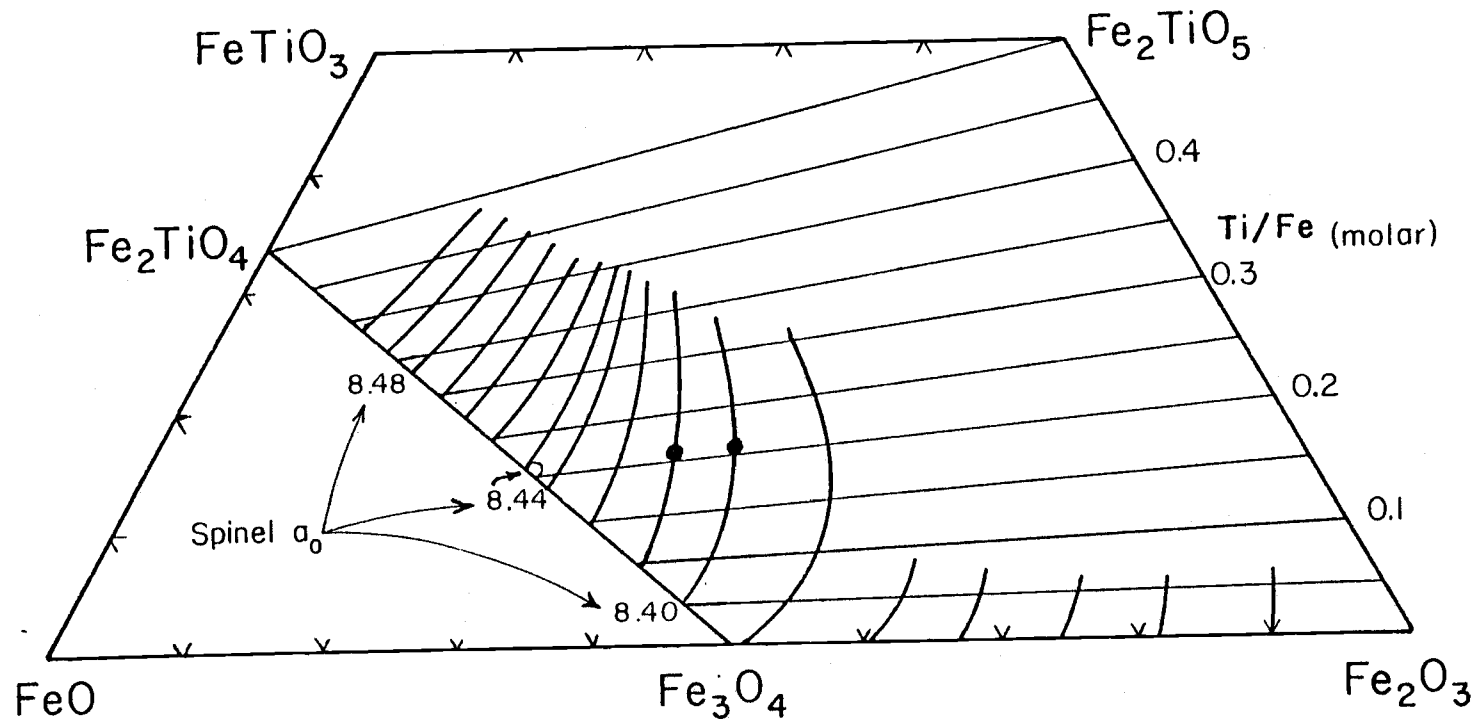


Figure 21: FeO - TiO<sub>2</sub> - Fe<sub>2</sub>O<sub>3</sub> diagram modified from Buddington and Lindsley, (1964). Shown are the initial ulvospinel content (open circle) and post-eruption oxidation (closed circles) for two samples of Tumalo tuff titanomaghemite.

Apatite occurs as inclusions in nearly all non-opaque phenocrysts and can occupy up to 15% of some hypersthene. The mixed pumice dacite contains trace ammounts of free acicular apatite microphenocrysts, which range in length up to 0.1 mm. Trace amounts of clear euhedral zircons are also found in the B-T and dacitic pumices.

## GEOCHEMISTRY

## 5.1 General Concepts

Crystallization of the B-T rhyodacite and mixed pumice dacite melts is assumed to have involved fractional crystallization; crystals were removed from contact with the melts as soon as they formed. The effects of crystal fractionation on trace element concentrations are evaluated through the Rayleigh Fractionation Law (Gast, 1968):

$$\text{Equation 1: } C_1 = C_0 F^{(D - 1)}$$

where:  $C_0$  = Element concentration in the parent melt

$C_1$  = Element concentration in the evolved melt

$F$  = Fraction of melt remaining after crystallization

$D$  = Bulk distribution coefficient;  $\sum X_i Kd_i$  where:

$X_i$  = Fraction of mineral  $i$  crystallizing

$Kd_i$  = Mineral $_i$  / Melt distribution coefficient

Distribution coefficients ( $Kd$ 's) which measure the ability of a mineral to incorporate an element into the crystal lattice are dependent on the composition and temperature of the melt, especially for high silica magmas (Mahood and Hildreth, 1983). For some minerals an increase of 10% silica can shift the  $Kd$  from significantly  $<1$  to significantly  $>1$ , changing the mineral from

trace-element incompatible to trace-element compatible. It is therefore important to use mineral  $K_d$ 's obtained from a system with a composition as close as possible to the modeled system. Distribution coefficients used in modeling the dacitic and rhyodacitic systems in this thesis are given in appendix 1, and shown graphically in figure 22.

Chondrite normalization of minor and trace element data corrects for the lower abundances of odd atomic numbered elements due to the Oddo-Harkins effect and emphasises variations in elemental abundances produced through geologic processes. Chondrite-normalized plots used in this thesis were calculated from C-1 chondrite concentrations given in Anders and Ebihara (1982) and are shown in appendix 2.

Many of the arguments in this chapter will focus on the geochemical behavior of the rare earth elements (REE). The REE La to Lu have atomic radii within 15% of each other and generally have a trivalent charge. They will therefore behave similarly under most geologic environments, with two notable exceptions. Under reducing conditions Eu will be divalent instead of trivalent and can be fractionated from the rest of the REE by Ca-bearing minerals (Weill and Drake, 1973). Under extremely oxidizing conditions Ce will be tetravalent and thus can be fractionated from the other trivalent REE.

All minor and trace element concentrations were obtained through the I.N.A.A. procedure outlined in chapter 1. Accuracies for these data are given at a 1 standard deviation confidence level unless otherwise stated. Uncertainties correspond to experimental errors



# DACITIC MINERAL /MELT DISTRIBUTION COEFFICIENTS

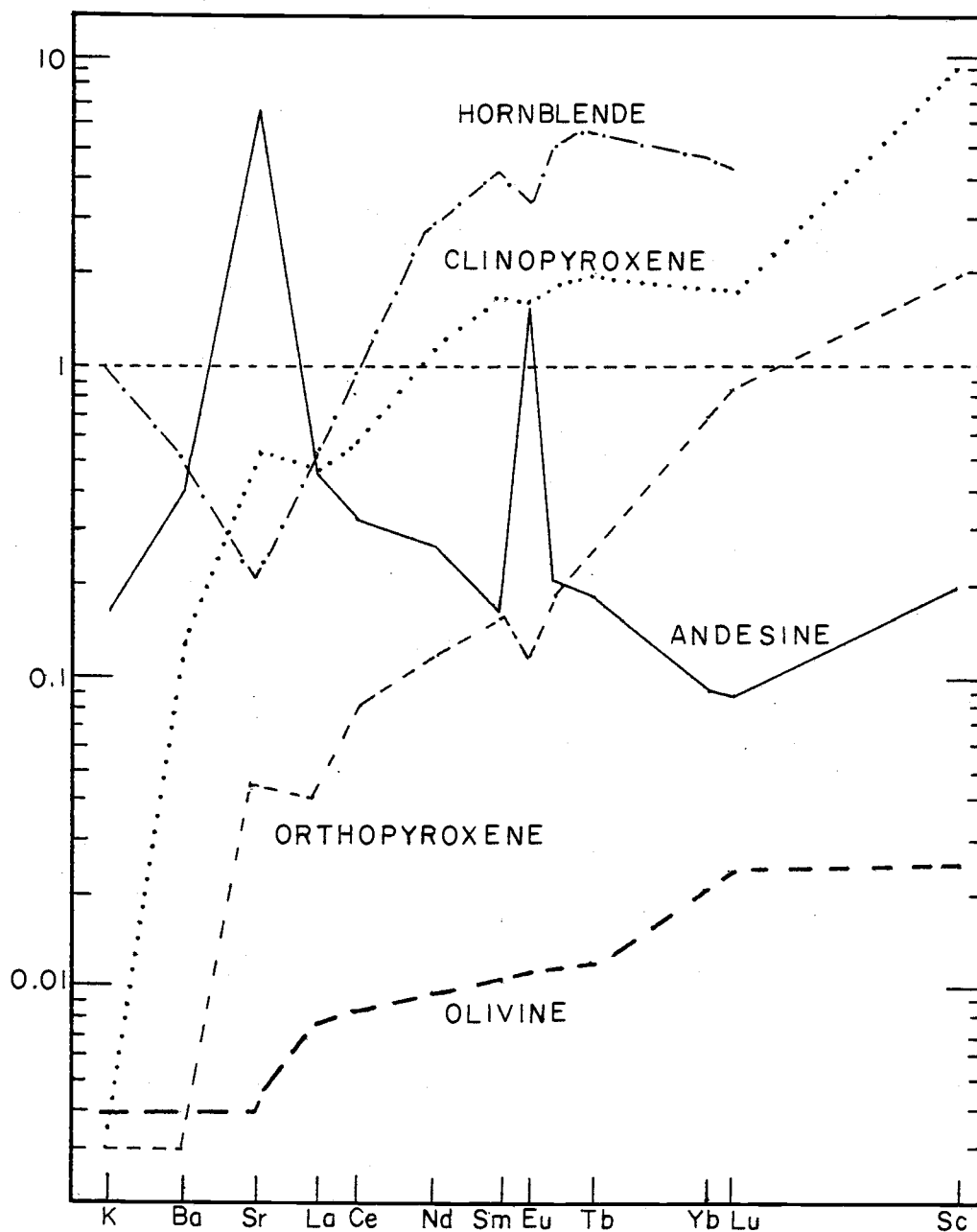


Figure 22: Mineral / Melt distribution coefficients used in geochemical models. Numerical data given in appendix 1.

and account for precision in replication of standards. Higher uncertainties correspond to lower elemental abundances when a range of uncertainty is given.

## 5.2 Bend Pumice Geochemistry

The Bend pumice is a peraluminous rhyodacite, having an average of 74% silica and less than 3.4% potash. Chemical abundances and sample locations for all analyzed Bend pumice samples are given in appendix 3. Selected sample analyses, with C.I.P.W. norms, and an average of 16 pumice analyses are given in table 3.

Samples 9111B and 9111C (table 3) represent the respective base and top of a six-meter-thick Bend pumice section located southwest of Laidlaw Butte. These two samples also represent the chemical extremes of 16 Bend pumice analyses; no systematic variations in chemistry with stratigraphic position have been observed in any analyzed Bend pumice section. Regular chemical variations with height in the air-fall section should be present if the Bend pumice was erupted from a chemically zoned or graded magma chamber. Comparing sample 9111B with 9111C results in a slight apparent zonation of major and trace elements in the Bend pumice section and appears to indicate that the Bend pumice magma chamber was zoned. The zonation also appears to be inverted relative to other well-known examples, with the more incompatible elements REE, Sc, Ba and Hf being enriched in the later-erupted pumice (9111C). Before zoning

Major Element Oxides (%)						
	8221B	8201A	9111R	9111C	BP Avg.	Unc(%)
SiO <sub>2</sub>	55.6	73.4	74.4	72.6	74	2-4
TiO <sub>2</sub>	1.09	0.13	0.13	0.18	0.14	5-20
Al <sub>2</sub> O <sub>3</sub>	19.9	15.0	12.9	14.0	14	5-10
FeO	7.3	1.8	1.8	2.2	1.9	1-5
MgO	4.2	Tr	0.1	0.2	0.1	5-40
CaO	7.5	0.8	0.8	1.0	0.9	2-11
Na <sub>2</sub> O	3.9	5.1	4.8	4.7	4.9	1-5
K <sub>2</sub> O	0.9	3.3	3.4	3.6	3.4	2-6
TOTAL	100.4	99.6	98.4	98.5	99.3	
Minor and Trace Elements (ppm)						
Sc	20.2	4.6	4.6	4.7	4.5	1-3
Cr	63*	7*	0.5	0.5	1	8-20
Co	228*	251*	0.58	0.56	0.55	1-9
Ni	21	4	1	1	3	20-50
Rb	22	92	63	61	67	8-20
Sr	630	40	48	48	56	9-40
Cs	1.03	3.0	2.9	2.7	2.8	3-7
Ba	580	940	760	810	780	7-9
La	20.4	29.4	28.7	30.7	29.7	1-2
Ce	36	62	57	59	60	1-5
Nd	19	26	23	26	26	5-30
Sm	5.57	5.91	6.00	6.17	6.1	1-2
Eu	1.69	0.63	0.68	0.87	0.77	1-2
Tb	0.70	0.97	0.95	0.99	0.96	3-5
Yb	3.0	4.2	4.3	4.4	4.3	2-7
Lu	0.36	0.62	0.69	0.73	0.69	2-6
Zr	110	160	170	170	170	15-20
Hf	3.4	6.7	6.7	7.0	6.8	2-3
Ta	2.5*	4.4*	1.23	1.24	1.24	2-5
Th	2.4	8.9	8.6	8.3	8.0	3-5
U	0.6	3.3	2.4	2.5	2.5	10-40
Normative Mineralogy						
Qtz	2.7	27.9	30.4	27.5	29.0	
Or	5.1	19.7	20.1	21.2	20.1	
Ab	33.0	43.1	40.6	39.8	41.5	
An	34.2	4.0	3.6	5.0	4.3	
Cor	0	1.5	0.1	0.6	0.3	
Di-Hd	2.5	0	0.33	0	0	
En-Fs	20.9	3.13	3.1	4.2	3.6	
Mgt	0.1	0.04	0.04	0.04	0.04	
Ilm	2.1	0.2	0.2	0.3	0.3	

Table 3: Bend pumice chemical abundances and C.I.P.W. normative mineralogies. \* denotes metal alloy contamination.

can be proved, uncertainties in the element concentrations must be accounted for. At the limits of one standard deviation, all elemental abundances in 9111B and 9111C overlap with the exception of Sc, La, Sm and Eu. At the limits of two standard deviations, all abundances overlap with the exception of Eu. Thus the only clear zoning in the Bend pumice section is shown by Eu, which is depleted in the earlier erupted pumice (9111B). Eu depletion in the upper part of the Bend pumice magma chamber can be accounted for with 3-5% plagioclase fractionation from an average Bend pumice composition. When statistical uncertainties are accounted for it does not appear that the Bend pumice is significantly zoned nor were there appreciable chemical gradients in the Bend pumice magma reservoir.

Perlitic obsidian (Sample 8201A) from the Bend pumice lower reworked zone has a composition which is almost identical to the Bend pumice, although it is more depleted in Sr and Eu and enriched in Ba, Rb, and Th (table 3). Enrichments of Co, Cr, and Ta in the obsidian are due to slight contamination by a metal alloy during sample preparation. The average Bend pumice and obsidian compositions are shown in a chondrite normalized plot in figure 23, which further shows the extent of Sr and Eu depletion. Fractionation of approximately 7% plagioclase from an average Bend pumice composition will produce the observed Sr and Eu depletions in the obsidian as well as enriching the obsidian in Ba, Rb, and Th.

Chemical evidence supports the interpretation that the perlitic obsidian in the lower reworked zone represents fragments of a small dome or plug, which was emplaced over the source vent prior to the

Figure 23: Chondrite-normalized plot of selected Bend pumice samples. The average composition of the Bend pumice, perlite obsidian (8201A), and a basaltic andesite rock fragment (8221B) are shown.

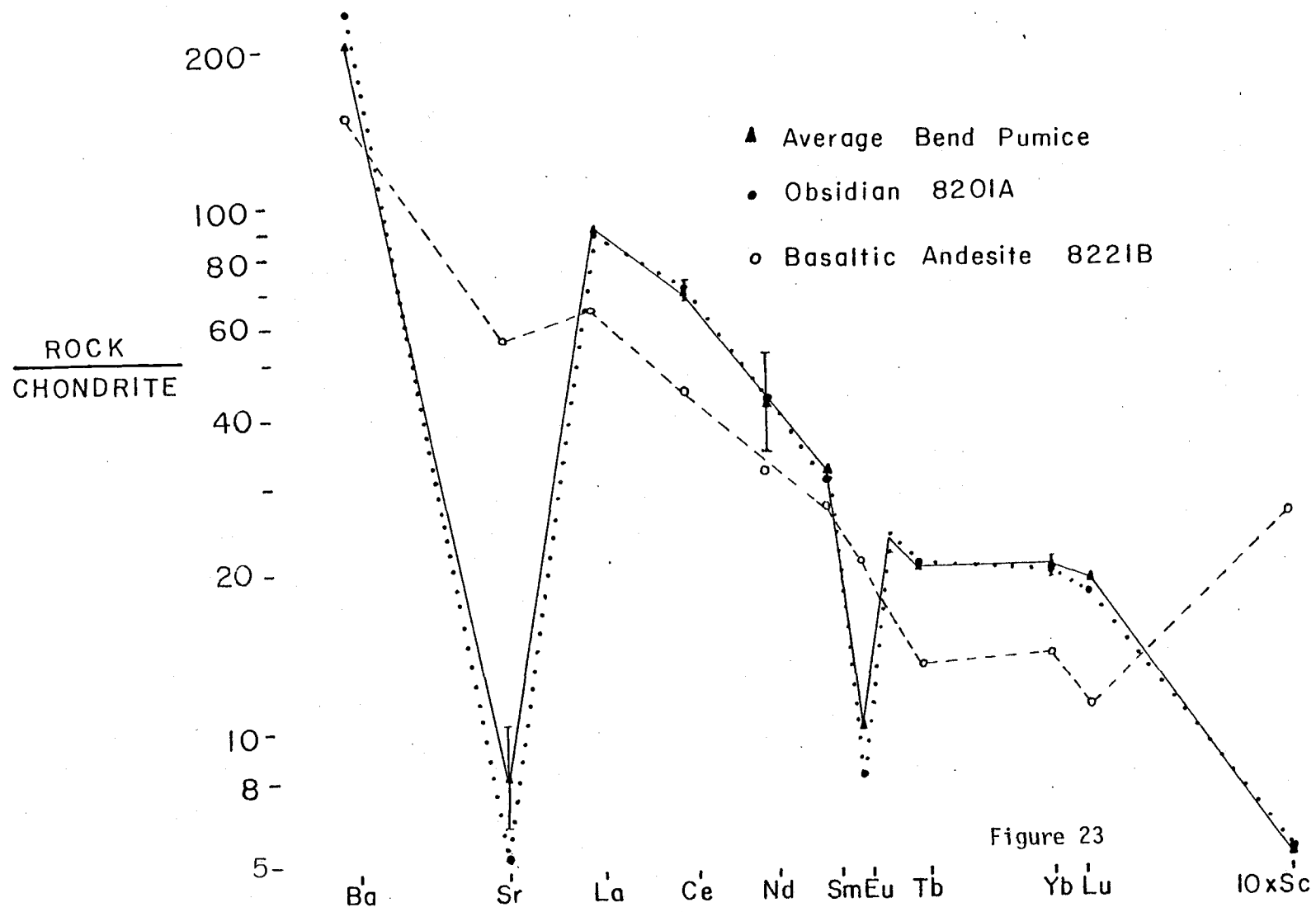


Figure 23

main Bend pumice eruption. The obsidian composition indicates that a batch of the Bend pumice rhyodacitic magma resided below the vent for at least a short interval of time, in order to allow plagioclase fractionation and emplacement of the obsidian. This magma could not have equilibrated under near-surface oxidizing conditions as had other rhyodacites analyzed by Hughes (1982), because Eu is only fractionated from the rest of the REE under reducing conditions.

A basaltic andesite rock fragment from the Bend pumice (sample 8221B, table 3) was also analyzed. Because basaltic andesite is thought to be a parental magma for the central High Cascade silicic series (Hughes, 1982), sample 8221B was modeled to see if a reasonable path of crystal fractionation existed toward the Bend pumice rhyodacite. Using sample 8221B as the starting composition POAM (Plagioclase-Orthopyroxene and Olivine-Augite-Magnetite) fractionation, which has been used in models to derive other central High Cascade silicic magmas (Hughes, 1982), is incapable of producing the observed depletions of Sr and Eu in the Bend pumice rhyodacite. While it is possible to appeal to more complex fractionation and assimilation models for deriving the Bend pumice rhyodacite from this basaltic andesite parent, it is more likely that sample 8221B is a xenolith and does not lie along a common path of magmatic evolution with the Bend pumice.

### 5.3 Tumalo Tuff Geochemistry

The Tumalo tuff is also a peraluminous rhyodacite, having an average of 75% silica and 3.6% potash. Chemical abundances and sample locations for analyzed Tumalo tuff samples are given in appendix 4. Averages for three Tumalo tuff rhyodacitic pumices and rhyodacitic pumice zones from Tumalo tuff mixed pumices are given in table 4.

The Tumalo tuff has undergone post-emplacement vapor-phase alteration, where the only visible effect has been the hydration and oxidation of iron oxide in the glass. Analysis of sample 753E (appendix 4), which is from the highly altered rim of a Tumalo tuff pumice block, shows that within the limits of analytical uncertainty the major elements remained immobile during vapor-phase alteration. The alteration was probably produced through the heating of moist air which had been ingested into the ash flow. The ingested air mixed with a relatively minor amount of corrosive magmatic gas, which had evolved from the glass, and produced the weak alteration present in the tuff.

The Bend pumice and Tumalo tuff rhyodacites do not appear to show significant differences in chemical abundances. At a 95% confidence level, one-way analysis of variance between the two sample populations also fails to show real chemical differences between the Bend pumice and Tumalo tuff. Chemical evidence thus supports the mineralogical and field interpretations that the Bend pumice and Tumalo tuff are the products of a common magma chamber. The lack of



Major Element Oxides (%)					
	TT avg.	Mrd avg.	Rd avg.	Mdac avg.	Unc(%)
SiO <sub>2</sub>	74	74	75	66.1	2-4
TiO <sub>2</sub>	0.15	0.16	0.15	0.91	3-10
Al <sub>2</sub> O <sub>3</sub>	14.8	15	15	17	6-10
FeO	2.0	2.0	2.0	5.6	3-5
MgO	0.1	0.1	0.1	1.4	5-50
CaO	0.85	0.89	0.87	3.6	3-5
Na <sub>2</sub> O	4.7	4.5	4.6	5.2	2-5
K <sub>2</sub> O	3.5	3.6	3.6	1.90	3-5
TOTAL	99.00	100.25	100.40	101.71	

Minor and Trace Elements (ppm)					
Sc	4.6	4.7	4.7	12.4	1-3
Cr	1	2	1	13	30-50
Co	0.52	0.6*	0.54*	6**	3-17
Ni	2	3	2	8	25-50
Rb	75	75*	75*	46**	9-17
Sr	58	70	65	305	13-20
Cs	2.8	2.9*	2.9*	1.8**	4-6
Ba	880	842*	853*	729**	3-7
La	30.1	30.2*	30.2*	27.9**	1-3
Ce	63	63*	63*	61**	1-6
Md	24	28*	27*	32**	9-18
Sm	6.2	6.2*	6.2*	7.8**	2-4
Eu	0.77	0.77*	0.77*	1.99**	1-8
Tb	1.00	1.03*	1.02*	1.03**	3-5
Yb	4.4	4.3*	4.3*	4.3**	2-7
Lu	0.69	0.68*	0.68*	0.67**	2-7
Zr	170	170	170	159	5-7
Hf	7.2	7.0*	7.6*	6.5**	2-3
Ta	1.28	1.36*	1.34*	1.13**	2-5
Th	8.2	8.0*	8.2*	5.2**	3-5
U	2.6	2.6*	2.9*	1.9**	10-20

Table 4: Tumalo tuff chemical abundances. TTavg = Average of 3 rhyodacitic pumices (samples 734D, 3234, 3245). Mrd = average of 4 mixed pumice rhyodacitic zones (6291S, 4172S, 3235S, 3245S); \* = includes samples BHT(1,3,5,7). rd avg = average of all Tumalo tuff rhyodacitic pumices. Mdac = average of 4 mixed pumice dacite zones (6291M, 4172M, 3235M, 3245M); \*\* = includes samples BHT(2,4,6).

significant compositional changes between the Bend pumice and Tumalo tuff further indicates that there was no appreciable hiatus between eruption of these two units.

Data presented by Hughes (1982) indicates that other High Cascade rhyodacites are the products of extensive crystal fractionation in shallow-level magma chambers, usually involving plagioclase + clinopyroxene + orthopyroxene + magnetite + apatite fractionation. These rhyodacites characteristically exhibit large variations in HREE abundances due to variable amounts of pyroxene fractionation. Low La to Ce ratios are usually present due to the assumed oxidation of Ce to a tetravalent state under shallow-level conditions. Tetravalent Ce will then behave incompatibly with the rest of the REE and will not be incorporated into REE-compatible minerals such as apatite (Hughes, 1982). Low La to Ce ratios may also be produced through La fractionation (Dr. R. A. Schmitt, pers. comm.). Large negative Eu anomalies are rarely present in the analyzed High Cascade rhyodacites of Hughes (1982), because Eu will remain in a trivalent state under assumed shallow-level oxidizing conditions (Weill and Drake, 1973).

In the B-T rhyodacite, none of the chemical features associated with shallow-level fractionation are present. Major depletions of Sr and Sc (figure 23) and  $\text{FeO} / \text{FeO} + \text{MgO}$  molar ratios  $> 0.9$  indicate that the B-T rhyodacite is a product of extensive fractionation. Large negative Eu anomalies and relatively higher La to Ce ratios indicates that the B-T magma evolved under more reducing conditions than other analyzed High Cascade rhyodacites. While the presence of hornblende

in the B-T rhyodacite suggests that at least 2%  $H_2O$  must have been in the melt, depths must have been sufficient to keep the magma at  $fO_2$  low enough for Eu and Ce (?) to have remained in reduced states. These depths cannot be accurately determined for the B-T rhyodacite, based on the available data. Chemical and mineralogical evidence presented does not support shallow-level fractionation as a viable mechanism for producing the B-T rhyodacite.

Without knowing the possible depths of crystallization, it is difficult to constrain the minerals which could have fractionated from the B-T rhyodacitic parent. Major depletions of Sr and Eu in the B-T rhyodacite could be due to plagioclase fractionation, while Sc depletion may be due to fractionation of pyroxene or amphibole. Other relatively high-magnesian minerals such as olivine must have fractionated from the B-T parental magma, to account for  $FeO / FeO+MgO$  molar ratios  $>0.9$ .

#### 5.4 Mixed Pumice Geochemistry

Mixed pumices (figure 19) which preserve the incomplete mixing between two different magmas are found in proximal Tumalo tuff exposures. Elemental abundances and sample locations for Tumalo tuff mixed pumice samples 4172, 6291, 3245, 3235 (S= rhyodacitic, M= dacitic) and BHT 1-6 are given in appendix 4, with average compositions of these samples given in table 4. Chondrite normalized trends for the dacitic and rhyodacitic pumice zones in the mixed

pumices are shown in figure 24.

The Tumalo tuff mixed pumices consist of a rhyodacite ( $\text{SiO}_2 = 74\%$ ,  $\text{K}_2\text{O} = 3.6\%$ ) intermingled with a black, peraluminous dacite ( $\text{SiO}_2 = 66\%$ ). As shown in table 4, the mixed pumice rhyodacite has the same composition as the B-T rhyodacite and will be referred to as B-T rhyodacite hereafter.

The formation of mixed pumices is generally attributed to mixing between compositionally distinct layers of a zoned magma chamber (Smith, 1979; Blake, 1981). Two processes are reasonably capable of producing a compositionally zoned magma chamber from an initially homogeneous magma. They are thermogravitational diffusion and crystal fractionation. These processes were tested for the Tumalo tuff mixed pumices to see if the contrasting pumice types were possibly produced through thermogravitational diffusion or crystal fractionation.

Thermogravitational diffusion (Hildreth, 1979) is a complex diffusion processes which incorporates

"...convective circulation, internal diffusion, complexation, and wall rock exchanges to develop compositional gradients, which are linked to gradients in the structure of the melt and are controlled by the thermal and gravitational fields of the magma chamber itself." (Hildreth, 1979)

Thermogravitational diffusion is capable of explaining large variations in trace element abundances which cannot be accounted for through crystal fractionation.

Previous studies involving thermogravitational diffusion have focused on large caldera complexes such as that producing the >170

Figure 24: Chondrite-normalized plot of the average of 7 Tumalo tuff rhyodacitic pumice zones and the average of 7 dacitic pumice zones from the Tumalo tuff mixed pumices. Error bars represent 1 standard deviation and are shown when uncertainty is greater than the size of the plotted data point.

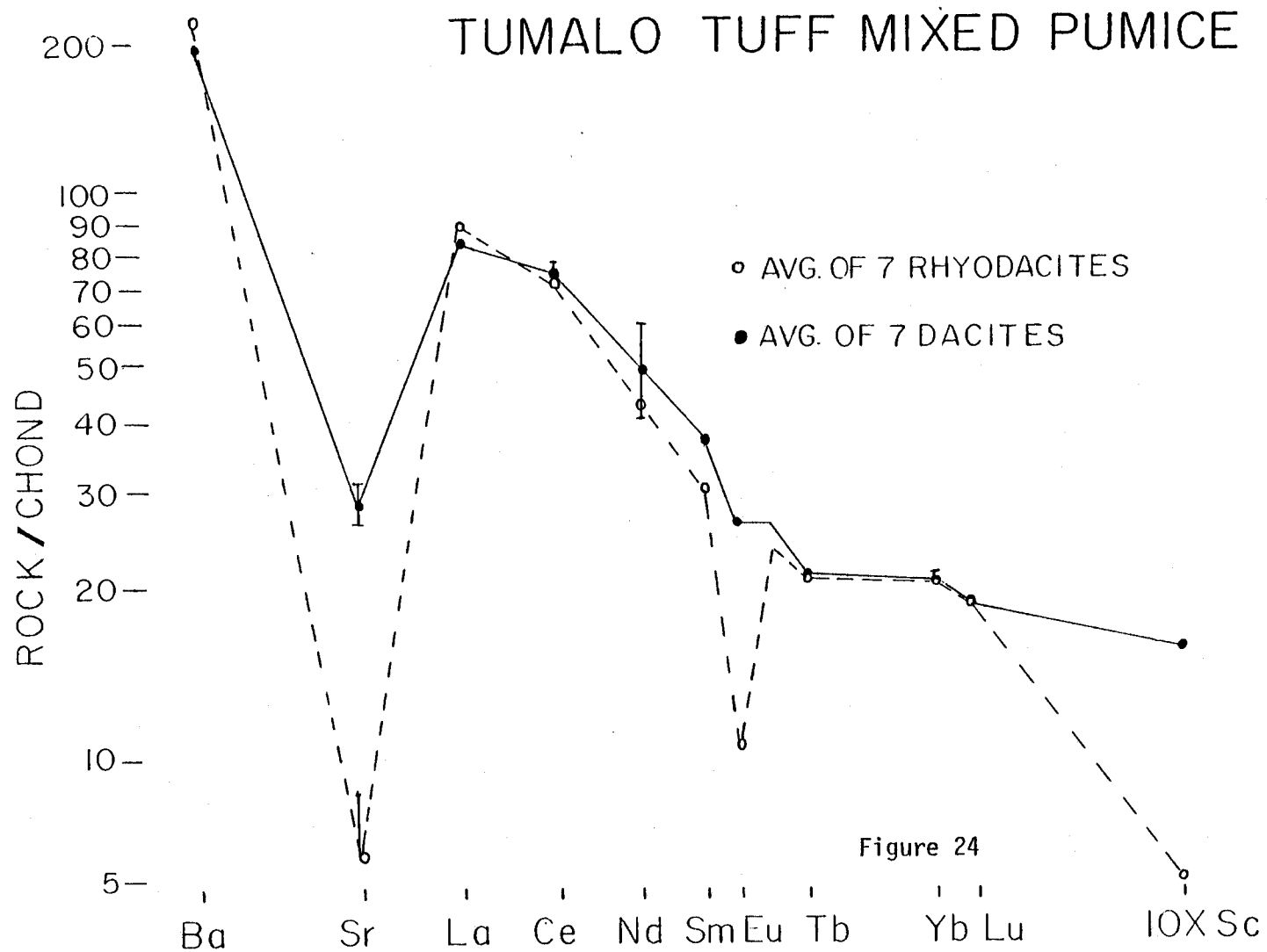


Figure 24

km<sup>3</sup> Bishop Tuff. These large systems involve magma volumes approximately two orders-of-magnitude greater than the B-T eruption. However, smaller-volume magma systems will tend to form temperature and compositional gradients more rapidly than large-volume systems because a small-volume system will have a larger surface-to-volume ratio, resulting in a greater heat loss per unit time (Spera, 1983). Smaller-volume systems should thus show the effects of thermogravitational diffusion more rapidly than larger-volume systems, if thermogravitational diffusion operates on the system.

As shown earlier in this work, the Bend pumice does not contain significant compositional gradients, nor are there significant chemical differences between the Bend pumice, Tumalo tuff, and the mixed pumice rhyodacite. At least 1 km<sup>3</sup> of magma was erupted to produce the Bend pumice and Tumalo tuff, which probably represents at least 10% of the total volume of the magma chamber (Smith and Shaw, 1975). If the dacitic and rhyodacitic compositions in the Tumalo tuff mixed pumice were produced through thermogravitational diffusion some chemical gradients should be present in the tephra erupted before the mixed pumices. Even if the top of the B-T magma chamber was homogenized, some sort of a chemical gradient should have been preserved in the Bend pumice before the dacitic magma was abruptly tapped in an assumed deeper level of the magma chamber. The lack of such gradients leads to the conclusion that thermogravitational diffusion did not produce a zoned B-T magma chamber which was then mixed to form the Tumalo tuff mixed pumices.

The other mechanism capable of producing a zoned magma chamber

from an initially homogeneous melt is crystal fractionation. If crystal fractionation produced a zonation in the B-T magma chamber, then the mixed pumice dacite and B-T rhyodacite must lie along a common path of fractionation. The B-T rhyodacite and dacite were modeled using Rayleigh fractionation. The mineral assemblage used was Plag + Cpx + Opx + Hb + Ol + Mgt + (Ap, All, Zr), with corresponding dacitic mineral  $k_d$ 's given in appendix 1.

From figure 24, it is apparent that crystal fractionation must maintain a constant concentration of HREE. Evaluation of Equation 1 shows that the bulk distribution coefficient,  $D$ , must equal 1 for the HREE. HREE-compatible hornblende is thus limited to <20% of the crystallizing assemblage and clinopyroxene to <60%; Yb  $k_{d_{hb}} = 4.89$ , multiplied by approximately 20% equals 1, which equals the maximum allowable  $D$  for Yb. Large amounts of plagioclase must also be fractionated from the dacite, to produce the observed depletions of Eu in the B-T rhyodacite. With hornblende limited to <20%, at least 50% of the initial dacitic melt must be crystallized using 80% Plag and 20% Hb to produce the rhyodacite Eu concentration. Including any other mineral in the crystallizing assemblage will lower the  $D$ , and thus increase the amount of crystallization the dacite must have undergone. The dacite must have thus undergone a minimum of 50% crystallization to have produced the observed Eu concentration in the B-T rhyodacite.

Both the dacite and the B-T rhyodacite have similar LREE concentrations. The LREE La is incompatible in all minerals, with the exception of the trace minerals apatite and allanite. Excluding



these trace minerals, it is not possible to have crystallized more than 13% of the dacite and still produce the observed concentrations of La in the B-T rhyodacite. The same argument applies to the LREE Ce, which further limits the maximum amount of dacite crystallization to <15%. Thus any amount of dacite crystallization beyond 13-15% would increase the modeled LREE concentrations above what is observed in the B-T rhyodacite.

The trace minerals apatite and allanite have large  $K_d$ 's for the LREE. Crystallizing small amounts of apatite and allanite could lower the LREE concentration, if >15% of the dacitic melt were crystallized. Elements with  $K_d$ 's similar to and greater than the LREE in apatite and allanite (Th, Hf, and Ta) are all enriched in the B-T rhyodacite; if apatite and allanite were fractionated from the dacite these elements should be depleted in the B-T rhyodacite. Trace minerals thus cannot be used to lower the LREE concentration in the rhyodacite and the maximum amount of crystallization the dacitic magma could have undergone is limited to < 15%. This amount of crystallization is insufficient to produce the observed depletion of Eu in the B-T rhyodacite.

The disparity between LREE, Eu, and constant HREE concentrations shows best that the mixed pumice dacite and B-T rhyodacite are not related by a common path of crystal fractionation. Modeling the trace elements Sc, Sr and Ta also shows a large disparity between the amount of crystallization necessary to evolve the rhyodacite from the dacite and the maximum amount of crystallization permitted by the observed elemental abundances.

It is thus not possible for the B-T magma chamber to have been zoned through either thermogravitational diffusion or crystal fractionation. The mixing of a zoned magma chamber could not have produced the Tumalo tuff mixed pumices. Neither could the dacite and B-T rhyodacite have evolved along a common path of crystal fractionation, been separated, and then re-mixed during the B-T eruption.

Assimilation of dacitic country rock by the B-T rhyodacite could not have produced the mixed pumice dacite. The dacite was completely molten when it was mixed with the B-T rhyodacite and a rhyodacitic melt lacks sufficient heat to completely melt dacitic xenoliths or wall rocks. The homogeneity of the B-T rhyodacite and its large volume relative to the dacite precludes formation of the rhyodacitic magma through large-scale assimilation of silicic country rocks by the dacitic magma.

The model which best fits the available data for the Tumalo tuff mixed pumices is that in which the dacite was from a separate magma source and was injected into the B-T rhyodacitic magma reservoir at some point just prior to, or during, the B-T eruption. While it may be possible that the dacitic magma resided in the B-T magma reservoir for a short interval of time prior to the eruption, it is more likely that invasion of dacitic magma into the rhyodacitic reservoir would have increased the gas content of the magma chamber and triggered an eruption (Huppert et al., 1982). While the dacite and B-T rhyodacite may have once had a common parental magma such as basaltic andesite, they must have evolved along different paths. These divergent paths

may have included multiple episodes of crystal fractionation, magma mixing and crustal assimilation, all occurring under variable physical conditions.

The mixing of magmas from unrelated sources is generally dismissed in the geologic literature as unlikely and fortuitous (e.g. Smith, 1979; Anderson, 1980; McBirney, 1980). While the mixing of genetically unrelated magmas may indeed be fortuitous, it occurred during the B-T eruption and resulted in the formation of the Tumalo tuff mixed pumices.

## SUMMARY AND CONCLUSIONS

The Bend-Tumalo eruption occurred at least 0.89 but no later than 2.6 m.y.b.p. during a period of normal magnetic polarity. Detailed grain size analysis of the air-fall Bend pumice shows that the eruptive vent was probably located 15 to 20 km west of Bend, possibly coincident with the location of the present silicic highland. As the Bend-Tumalo eruption involved a minimum of  $1 \text{ km}^3$  of silicic magma, the vent was probably a large stratovolcano.

The eruption was initiated with the fragmentation of an obsidian dome which resided over the vent. Air-fall pumice deposits associated with the initial phase of the eruption were reworked and in places removed by erosion. A hiatus of uncertain, although probably short, duration occurred before the main stage of the eruption. The main stage of the B-T eruption produced the air-fall Bend pumice. Reverse grading in the Bend pumice was probably produced by increased diameter of the vent and reflects continuous eruption of the Bend pumice. The eruption culminated in collapse of the eruption column, which generated the Tumalo tuff ash flow. The Tumalo tuff was immediately emplaced over the Bend pumice, leaving the air-fall deposit without a characteristic graded top. The Tumalo tuff presumably traveled off the highland and was channeled by a northeast-trending drainage system, giving the appearance of a southwest-to-northeast dispersal pattern. Column collapse was

probably initiated by widening of the vent to a point where the upward flow from the vent could not support the mass of the eruption column. Widening of the vent beyond this critical diameter may have been caused by the invasion of dacitic magma into the erupting reservoir, as mixed pumices are found in proximal Tumalo tuff deposits. The dacitic magma could have increased the eruption rate, which would have rapidly increased erosion of the vent walls. Invasion of dacitic magma into the erupting reservoir is not a prerequisite for initiating column collapse.

In the B-T rhyodacitic pumices sodic andesine and high iron ferrohypersthene indicate that the B-T magma was more highly evolved than other reported central High Cascade rhyodacites. Fresh unresorbed hornblende also indicates that hydrous B-T magma evolved at depths greater than 10 km, with no significant residence time in a near surface magma reservoir prior to eruption.

The presence of fresh hornblende in the mixed pumice dacite shows that this magma also evolved at depth and under hydrous conditions similar to the B-T rhyodacite. While the high abundance of hornblende is anomalous, other mineralogical features in the mixed pumice dacite are typical of High Cascade dacites.

Both the Bend pumice and the Tumalo tuff are peraluminous rhyodacites and have nearly identical major, minor, and trace element abundances. The only chemical inhomogeneities in the Bend pumice are apparently related to a roof zone in the magma chamber which had undergone 3-5% plagioclase fractionation; no chemical gradients are observed in the Bend pumice. Obsidian from the Bend pumice lower

reworked zone was produced through 7% plagioclase fractionation of the B-T rhyodacite and represents the remnants of a dome which was emplaced shortly before the B-T eruption. Major depletions of Eu and high La to Ce ratios in the B-T rhyodacite are unusual for a highly evolved High Cascade magma and probably indicates that the B-T rhyodacite did not evolve through crystal fractionation in a shallow-level magma chamber. This may indicate that the paleo-highland source of the Bend pumice and Tumalo tuff was under a different set of physical conditions than previously studied central High Cascade silicic magma sources, even though the two magma centers may have been less than 10 km apart.

Mixed pumices in the Tumalo tuff preserve incomplete mixing between B-T rhyodacite and a dacite. Trace element modeling fails to relate these two magmas through crystal fractionation or thermogravitational diffusion, nor can the magmas reasonably be related through assimilation of crustal rocks. The best explanation for the origin of the Tumalo tuff mixed pumices is mixing of two genetically unrelated magmas during the B-T eruption. The B-T rhyodacite and dacite may have originally had a common parental source but have since evolved under divergent physical conditions. The dacitic magma may have invaded the B-T magma reservoir shortly before the eruption, although injection of dacitic magma into a rhyodacitic reservoir would have rapidly triggered an eruption. Irregardless of when mixing occurred, it resulted in the formation of the Tumalo Tuff mixed pumices.

The mixing of genetically unrelated magmas from physically

separate sources should not be dismissed as a viable explanation for mixed pumice formation, nor as a possible explanation for contrasting magma types occurring around a common vent.

## REFERENCES

- Anders, D. and Ebihara, T. 1982, The chemical composition of C1 chondrites; a new estimate for pre-solar elemental abundances: *Geochim. Cosmochim. Acta* 46, 2363-2380.
- Anderson, A.T. 1976, Magma Mixing: Petrological process and volcanological tool: *J. Volc. Geotherm. Res.* 1, 3-33.
- . 1980, Significance of hornblende in calc-alkaline andesites and basalts: *Am. Mineral.* 65, 837-851.
- Arth, J.G. 1976, Behavior of trace elements during magmatic processes - A summary of theoretical models and their applications: *J. Res. U.S. Geol. Survey* 4, 41-47.
- Arth, J.G. and Barker, F. 1976, Rare earth partitioning between hornblende and dacitic liquid and implications for the genesis of trondhjemitic - tonalitic magmas: *Geology* 4, 534-536.
- Bagnold, R.A. 1954, Experiments on a gravity-free dispersion of large solid spheres in a Newtonian fluid under shear: *Proc. R. Soc. London A* 225, 49-63.
- Blake, S. 1981, Eruptions from zoned magma chambers: *J. Geol. Soc. London* 138, 281-287.
- Buddington, A.F. and Lindsley, D.H. 1964, Iron - titanium oxide minerals and synthetic equivalents: *J. Petrol.* 5, 310-357.
- Cannon, D.M. 1984, The stratigraphy, geochemistry and mineralogy of two ash-flow tuffs in the Deschutes Formation, central Oregon. Unpublished M.S. thesis, Oregon State University, Corvallis. 100 p.
- Dudas, M.J., Schmitt, R.A. and Harward, M.E. 1971, Trace element partitioning between volcanic plagioclase and dacitic pyroclastic matrix: *Earth Planet. Sci. Letters* 11, 440-446.
- Eichelberger, J.C. 1975, Origin of andesite and dacite: Evidence of mixing at Glass Mountain in California and at other circum-pacific volcanoes: *Geol. Soc. Amer. Bull.* 86, 1381-1391.
- . 1981, Mechanism of magma mixing at Glass Mountain, Medicine Lake Highland Volcano, California: In Johnston DA and Donnelly-Nolan J, eds., *Guides to some volcanic terranes in Washington, Idaho, Oregon, and Northern California*. U.S. Geol. Survey Circ. 838, 183-189.



- Fisher, R.V. 1964, Maximum size, median diameter, and sorting of tephra: *J. Geophys. Res.* 69, 341-355.
- , 1979, Models for pyroclastic surges and pyroclastic flows: *J. Volc. Geotherm. Res.* 6, 305-318.
- Fountain, J.C. 1979, Geochemistry of Brokeoff Volcano, California: *Geol. Soc. Amer. Bull.* 90, 294-300.
- Froggatt, P.C. 1982, Review of methods of estimating rhyolitic tephra volumes; Applications to the Taupo Volcanic Zone, New Zealand: *J. Volc. Geotherm. Res.* 14, 310-318.
- Gast, P.W. 1968, Trace element fractionation and the origin of tholeiitic and alkaline magma types: *Geochim. Cosmochim. Acta* 32, 1057-1085.
- Gill, J.B. 1978, Role of trace element partition coefficients in models of andesite genesis: *Geochim. Cosmochim. Acta* 42, 709-724.
- , 1981, *Orogenic andesites and plate tectonics*, Springer-Verlag, New York, 390 p.
- Gerlach, D.C. and Grove, T.L. 1982, Petrology of Medicine Lake Highland volcanics: Characterization of endmembers of magma mixing: *Contrib. Mineral. Petrol.* 80, 147-159.
- Guest, J.E. 1968, Banded pumice in a Chilean ignimbrite: *Geol. Mag.* 105, 177-184.
- Hanson, G.N. 1980, Rare earth elements in petrogenetic studies of igneous systems: *Ann. Rev. Earth Planet. Sci.* 8, 371-406.
- Helz, R.T. 1982, Phase relations and compositions of amphiboles produced in studies of the melting behavior of rocks: In Veblen DR and Ribbe PH eds., *Reviews in mineralogy*, 9B, Amphiboles: Petrology and experimental phase relations. *Amer. Mineral. Inst.*, 279-347.
- Hildreth, W. 1979, The Bishop Tuff: Evidence for the origin of compositional zonation in silicic magma chambers: *Geol. Soc. Amer. Sp. Paper* 180, 43-75.
- Hughes, S.S. 1982, Petrochemical evolution of the High Cascade volcanics in the Three Sisters region, Oregon: Unpublished PhD thesis, Oregon State University, Corvallis. 199 p.
- Huppert, H.E., Sparks, R.S.J., and Turner, J.S. 1982, Effects of volatiles on mixing in calc-alkaline magma systems: *Nature* 297, 554-557.

- Irving, A.J. 1978, A review of experimental studies of crystal/liquid trace element partitioning: *Geochim. Cosmochim. Acta* 42, 743-770.
- Jakeš, P. and White, A.J.R. 1972, Hornblendes from calc-alkaline volcanic rocks of island arcs and continental margins: *Am. Mineral.* 57, 887-902.
- Kerr, P.F. 1977, *Optical Mineralogy*, McGraw-Hill, New York, 492 p.
- Laul, J.C. 1979, Neutron activation analysis of geologic materials: *Atomic Energy Rev.* 17, 603-695.
- Lidstrom, J.W., Jr. 1971, A new model for the formation of Crater Lake caldera, Oregon: Unpublished PhD thesis, Oregon State University, Corvallis. 85 p.
- MacDonald, G.A. and Katsura, T. 1965, Eruption of Lassen Peak, Cascade Range, California, in 1915: Example of mixed magmas: *Geol. Soc. Amer. Bull.* 76, 475-482.
- MacLeod, N.S., Sherrod, D.R., and Chitwood, L.A. 1982, Geologic map of Newberry Volcano, Deschutes, Klamath, and Lake Counties, Oregon: U.S. Geol. Survey Open-File Report 82-847, 27p.
- Mahood, G. and Hildreth, W. 1983, Large partition coefficients for trace elements in high silica rhyolites: *Geochim. Cosmochim. Acta* 47, 11-30.
- McBirney, A.R. 1980, Mixing and unmixing of magmas: *J. Volc. Geotherm. Res.* 7, 357-371.
- Mimura, K. and MacLeod, N.S. 1978, Source directions of pumice and ash deposits near Bend, Oregon: *Geol. Soc. Amer. Abs. with Programs* 10, p. 137.
- Murase, T. and McBirney, A.R. 1973, Properties of some common igneous rocks and their melts at high temperatures: *Geol. Soc. Amer. Bull.* 84, 3563-3592.
- Nagasawa, H. and Schnetzler, C.C. 1971, Partitioning of rare earth, alkali, and alkaline earth elements between phenocrysts and acidic igneous magma: *Geochim. Cosmochim. Acta* 35, 953-968.
- O'Hara, M.J. 1977, Geochemical evolution during fractional crystallization of a periodically refilled magma chamber: *Nature* 266, 503-507.

- Peterson, N.V., Groh, E.A., Taylor, E.M. and Stensland, D.E. 1976, Geology and mineral resources of Deschutes County, Oregon: Or. Dept. Geol. Min. Ind. Bull. 89, 66 p.
- Schmid, R. 1981, Descriptive nomenclature and classification of pyroclastic deposits and fragments: Recommendations of the I.U.G.S. Subcommission on the Systematics of Igneous Rocks: Geology 9, 41-43.
- Sheridan, M.F. 1979, Emplacement of pyroclastic flows: A review: Geol. Soc. Amer. Sp. Paper 190, 125-136.
- Smith, G.A. and Priest, G.R. 1983, A field trip guide to the central Oregon Cascades: Oregon Geology 45, 119-126.
- Smith, G.A. and Taylor, E.M. 1983, The central Oregon High Cascades graben: What, Where, When: Geotherm. Resour. Council Trans. 7, 275-279.
- Smith, R.L. 1960, Zones and zonal variations in welded ash flows: U.S. Geol. Survey Prof. Paper 345-F, 149-159.
- , 1979, Ash flow magmatism: Geol. Soc. Amer. Sp. Paper 180, 5-27.
- Smith, R.L. and Bailey, R.A. 1966, The Bandelier Tuff: A study of ash-flow eruption cycles from zoned magma chambers: Bull. Volcanol. 29, 83-104.
- Smith, R.L. and Shaw, H.R. 1975, Igneous-related geothermal systems: In White DE and Williams DL eds., Assessment of geothermal resources of the United States - 1975, U.S. Geol. Survey Circ. 726, 58-83.
- Sparks, R.S.J. 1976, Grain size variations in ignimbrites and implications for the transport of pyroclastic flows: Sedimentology 23, 147-188.
- Sparks, R.S.J., Self, S. and Walker, G.P.L. 1973, Products of ignimbrite eruptions: Geology 1, 115-118.
- Sparks, R.S.J., Sigurdsson, H. and Wilson, L. 1977, Magma mixing: A mechanism for triggering acid explosive eruptions: Nature 267, 315-318.
- Sparks, R.S.J. and Wilson, L. 1976, A model for the formation of ignimbrites by gravitational column collapse: J. Geol. Soc. London 132, 441-451.
- Spera, F.J. 1983, Simulation of magma withdrawal from crustal reservoirs (abstr): Trans. Amer. Geophys. Union (EOS) 64, no. 45, p. 876.

- Taylor, E.M. 1978, Field geology of the southwest Broken Top quadrangle, Oregon: Or. Dept. Geol. Min. Ind. Sp. Paper 2, 50 p.
- \_\_\_\_\_, 1980, Volcanic and volcanoclastic rocks on the east flank of the central High Cascade Range to the Deschutes River, Oregon: Or. Dept. Geol. Min. Ind. Bull. 101, 1-7.
- \_\_\_\_\_, 1981, Central High Cascades roadside geology: Bend, Sisters, McKenzie Pass and Santiam Pass, Oregon: In Johnston DA and Donnelly-Nolan J, eds., Guides to some volcanic terranes in Washington, Idaho, Oregon, and Northern California. U.S. Geol. Survey Circ. 838, 55-62.
- Walker, G.P.L. 1971, Grain size characteristics of pyroclastic deposits: J. Geol. 79, 696-714.
- \_\_\_\_\_, 1981, Plinian eruptions and their products: Bull. Volcanol. 44-2, 223-240.
- \_\_\_\_\_, 1983, Ignimbrite types and ignimbrite problems: J. Volc. Geotherm. Res. 17, 65-88.
- Walker, G.P.L. and Wilson, C.J.N. 1983, Lateral variations in the Taupo ignimbrite: J. Volcanol. Geotherm. Res. 18, 117-133.
- Weill, D.F. and Drake, M.J. 1973, Eu anomaly in plagioclase feldspar: Experimental results and semiquantitative model: Science 180, 1059-1060.
- Williams, H. 1957, A geologic map of the Bend quadrangle, Oregon, and a reconnaissance geologic map of the central portion of the High Cascade mountains: Or. Dept. Geol. Min. Ind. Map, scales 1:125,000 and 1:250,000.
- Wilson, C.J.N. and Walker, G.P.L. 1982, Ignimbrite depositional facies: The anatomy of a pyroclastic flow: J. Geol. Soc. London 139, 581-592.
- Wilson, L. 1976, Explosive volcanic eruptions - III. Plinian eruption columns: Geophys. J. R. astr. Soc. 45, 545-556.
- Wilson, L., Sparks, R.S.J. and Walker, G.P.L. 1980, Explosive volcanic eruptions - IV. The control of magma properties and conduit geometry on eruption column behaviour: Geophys. J. P. astr. Soc. 63, 117-148.
- Wright, J.V. and Walker, G.P.L. 1977, The ignimbrite source problem: Significance of a co-ignimbrite lag fall deposit: Geology 5, 729-732.

Yoder, H.S., Jr. 1973, Contemporaneous basaltic and rhyolitic magmas:  
Am. Mineral. 58, 153-171.

## APPENDICES

ELEMENT	OLIVINE <sup>a</sup>	ORTHOPYROXENE <sup>b</sup>	CLINOPYROXENE <sup>c,d</sup>	HORNBLLENDE <sup>e</sup>	PLAGIOCLASE <sup>f</sup>	An40	An23
K	0.004	0.001	0.037	1*	0.17		0.23
Ba	0.004*	0.003	0.131	0.5*	0.42		0.92
Sr	0.004*	0.046	0.516	0.2*	6.5		24.3
La	0.007	0.04*	0.35*	0.5*	0.32		0.30
Ce	0.008*	0.082	0.50	0.899	0.23		0.22
Nd	0.009*	0.113	1.11	2.80	0.17		0.19
Sm	0.010	0.133	1.67	3.99	0.157		0.168
Eu	0.011	0.113	1.56	3.44	1.49		4.2
Tb	0.013*	0.215*	1.89*	5.84*	0.17		0.21
Yb	0.021	0.73	1.58	4.89	0.09		0.11
Lu	0.023	0.88	1.54	4.53	0.10		0.11
Sc	0.25	2*	9*	unkn	0.197		0.171

Appendix 1: Mineral/Melt distribution coefficients used in geochemical modeling. Data from:

a) Hughes (1982) Fo87 olivines from High Cascades basalts

b) Nagasawa and Schnetzler (1971) Hypersthene from Ata (I) dacite, SiO<sub>2</sub> = 68%.

c) Arth (1976) Averages from dacitic and rhyodacitic rocks.

d) Irving (1978) Experimental determinations on calcic pyroxenes.

e) Arth and Barker (1976) Dacitic hornblendes.

f) Dudas et al. (1971) An<sub>40</sub> = Mazama dacitic pumice, An<sub>23</sub> = Tumalo tuff rhyodacitic pumice

\* Denotes values extrapolated from the published data.

<u>ELEMENT</u>	<u>C1 Non Volatile Mass (ppm)*</u>
K	737
Sc	7.7
Sr	10.4
Ba	3.00
La	0.312
Ce	0.813
Nd	0.603
Sm	0.197
Eu	0.074
Tb	0.047
Yb	0.210
Lu	0.0323

Appendix 2; C1 chondrite elemental abundances. Calculated after  
Anders and Ebihara (1982), Table 1.

\* C1 abundances minus their average C and H<sub>2</sub>O contents; i.e.  
total C1 abundances X 1.32.



MAJOR ELEMENT OXIDES (%)						
	<u>9101H</u>	<u>9101G</u>	<u>9101D</u>	<u>9101C</u>	<u>9101B</u>	<u>9101A</u>
SiO <sub>2</sub>	73.4	74.1	73.8	72.9	73.9	75.4
TiO <sub>2</sub>	0.14	0.14	0.13	0.14	0.14	0.14
Al <sub>2</sub> O <sub>3</sub>	13.0	13.0	13.1	13.6	13.4	13.6
FeO	1.96	1.95	1.92	1.95	1.93	1.97
MgO	0.1	0.1	Tr	Tr	Tr	0.1
CaO	0.90	0.88	0.89	0.92	0.88	0.90
Na <sub>2</sub> O	4.8	5.1	4.8	4.8	5.1	4.9
K <sub>2</sub> O	3.5	3.5	3.5	3.5	3.4	3.4
TOTAL	<u>97.6</u>	<u>98.7</u>	<u>98.1</u>	<u>97.8</u>	<u>98.8</u>	<u>100.4</u>
MINOR AND TRACE ELEMENTS (PPM)						
Sc	4.5	4.5	4.4	4.4	4.4	4.5
Cr	<1	<1	<1	<1	<1	2
Co	0.64	0.57	0.51	0.54	0.50	0.51
Ni	4	<2	<2	2	<2	3
Rb	63	61	62	62	61	61
Sr	40	79	52	30	50	69
Cs	2.6	2.7	2.7	2.7	2.7	2.8
Ba	780	800	770	810	770	770
La	29.4	30.0	29.5	29.7	29.3	29.7
Ce	59	60	59	59	60	59
Nd	25	22	27	25	27	24
Sm	6.08	6.12	6.02	6.12	6.02	6.16
Eu	0.81	0.81	0.80	0.79	0.76	0.76
Tb	0.97	0.98	0.98	0.97	0.97	0.97
Yb	4.3	4.3	4.3	4.3	4.3	4.3
Lu	0.71	0.72	0.72	0.72	0.71	0.71
Zr	-	-	-	-	-	-
Hf	6.8	6.8	6.6	6.8	6.7	6.6
Ta	1.25	1.26	1.23	1.17	1.19	1.18
Th	7.9	8.1	7.9	7.9	8.1	8.0
U	2.4	2.4	2.1	2.3	2.3	2.2

### Appendix 3: Bend pumice geochemistry and sample locations.

9101H: Pumice quarry 0.7 km SE Tumalo State Park, SE1/4 SE1/4 S6, T17S, R12E, 10-50 cm below Bend pumice - Tumalo tuff contact.

9101G: a/a, 0.9 m below Bend pumice - Tumalo tuff contact.

9101D: a/a, 1.5 m " " "

9101C: a/a, 2.1 m " " "

9101B: a/a, 2.7 m " " "

9101A: a/a, 3.3 m " " "

	MAJOR ELEMENT OXIDES (%)					
	<u>9102A</u>	<u>9111C</u>	<u>9111D</u>	<u>9111G</u>	<u>9111H</u>	<u>9111J</u>
SiO <sub>2</sub>	75.4	72.6	73.4	73.8	75.7	74.0
TiO <sub>2</sub>	0.14	0.18	0.15	0.14	0.14	0.14
Al <sub>2</sub> O <sub>3</sub>	12.6	14.0	13.7	16.0	13.7	13.3
FeO	1.93	2.17	1.98	1.90	1.93	1.89
MgO	0.1	0.2	0.2	0.1	0.1	0.1
CaO	0.89	1.02	0.84	0.86	0.84	0.85
Na <sub>2</sub> O	5.1	4.7	4.7	4.8	4.7	4.8
K <sub>2</sub> O	3.2	3.6	3.4	3.3	3.4	3.3
TOTAL	99.2	98.5	98.3	100.8	100.5	98.4

	MINOR AND TRACE ELEMENTS (PPM)					
Sc	4.6	4.7	4.7	4.3	4.5	-
Cr	<1	<1	<1	1	2	-
Co	0.56	0.56	0.56	0.51	0.51	-
Ni	2	2	2	3	2	-
Rb	61	61	61	77	81	-
Sr	30	50	30	69	73	-
Cs	2.8	2.7	2.8	2.7	2.9	-
Ba	750	810	800	980	680	-
La	28.8	30.7	30.1	29.9	30.4	-
Ce	61	61	63	61	64	-
Nd	26	26	27	21	27	-
Sm	6.16	6.17	6.18	6.03	6.21	-
Eu	0.68	0.87	0.87	0.78	0.73	-
Tb	0.97	0.99	0.99	0.94	1.00	-
Yb	4.1	4.4	4.4	4.5	4.5	-
Lu	0.68	0.73	0.71	0.68	0.65	-
Zr	-	-	-	170	170	-
Hf	7.0	7.0	7.1	6.6	6.9	-
Ta	1.24	1.24	1.21	1.24	1.33	-
Th	8.4	8.3	8.3	7.7	8.1	-
U	2.4	2.5	2.4	2.4	2.5	-

## Appendix 3: cont.

9102A: Road cut 0.1 km NW of Deschutes River Ranch, SE1/4 SW1/4 S17, T16S, R12E, 10-50 cm below Bend pumice - Tumalo tuff contact.

9111C: Abandoned pumice quarry 1 km SW of Bend, NW1/4 SW1/4 S6, T18S, R12E, 10-50 cm below Bend pumice - Tumalo tuff contact.

9111D: a/a, 0.9 m below Bend pumice - Tumalo tuff contact.

9111G: a/a, 1.5 m " " "

9111H: a/a, 2.1 m " " "

9111J: a/a, 2.7 m " " "

MAJOR ELEMENT OXIDES (%)						
	<u>9111K</u>	<u>9111L</u>	<u>9111M</u>	<u>9111N</u>	<u>9111A</u>	<u>9111B</u>
SiO <sub>2</sub>	73.8	72.6	72.7	73.5	74.0	74.6
TiO <sub>2</sub>	0.14	0.14	0.14	0.14	0.14	0.13
Al <sub>2</sub> O <sub>3</sub>	13.5	14.2	14.3	13.4	13.1	12.9
FeO	1.89	1.90	1.87	1.87	1.96	1.80
MgO	0.1	Tr	0.1	Tr	0.1	0.1
CaO	0.84	0.81	0.82	0.80	0.89	0.82
Na <sub>2</sub> O	5.1	5.0	5.0	4.9	5.1	4.8
K <sub>2</sub> O	<u>3.1</u>	<u>3.2</u>	<u>3.2</u>	<u>3.2</u>	<u>3.2</u>	<u>3.4</u>
TOTAL	98.5	97.9	98.2	97.8	98.5	98.6

MINOR AND TRACE ELEMENTS (PPM)						
Sc	4.6	-	4.5	4.5	4.5	4.6
Cr	<1	-	1	1	<1	<1
Co	0.54	-	0.54	0.54	0.66	0.58
Ni	3	-	1	2	2	1
Rb	78	-	80	78	78	59
Sr	76	-	80	72	67	50
Cs	2.8	-	2.8	2.8	2.7	2.9
Ba	790	-	750	750	770	760
La	30.6	-	29.6	30.3	28.9	28.7
Ce	63	-	64	63	58	59
Nd	29	-	27	33	24	23
Sm	6.31	-	6.14	6.19	6.8	6.00
Eu	0.77	-	0.78	0.77	0.72	0.68
Tb	0.98	-	0.97	0.97	0.96	0.95
Yb	4.4	-	4.4	4.4	4.3	4.3
Lu	0.64	-	0.64	0.65	0.69	0.69
Zr	170	-	170	170	-	-
Hf	7.1	-	6.9	6.9	6.7	6.7
Ta	1.29	-	1.30	1.30	1.26	1.23
Th	8.0	-	8.0	8.0	7.8	8.6
U	-	-	-	-	2.5	2.4

## Appendix 3: cont.

9111K: a/a, 3.3 m below Bend pumice - Tumalo tuff contact.

9111L: a/a, 3.9 m " " "

9111M: a/a, 4.5 m " " "

9111N: a/a, 5.1 m " " "

9111A: a/a, 5.7 m " " "

9111B: a/a, Coarse-pumice lens in LRZ, 35 cm below LRZ-UAZ contact.

MAJOR ELEMENT OXIDES (%)		
	9122A	Uncertainty (%)
SiO <sub>2</sub>	71.9	2-4
TiO <sub>2</sub>	0.17	5-10
Al <sub>2</sub> O <sub>3</sub>	16.6	5-10
FeO	2.18	3-5
MgO	0.1	50
CaO	0.87	4-6
Na <sub>2</sub> O	4.4	1-5
K <sub>2</sub> O	3.4	1-3
TOTAL	99.6	
MINOR AND TRACE ELEMENTS (PPM)		
Sc	4.7	1-3
Cr	3	10-50
Co	1.6	5-10
Ni	3	20-50
Rb	77	8-12
Sr	90	15-35
Cs	1.6	5-10
Ba	940	2-6
La	31.1	1-2
Ce	71	1-5
Nd	22	5-30
Sm	6.31	1-2
Eu	0.75	1-2
Tb	0.95	1-2
Yb	4.3	2-5
Lu	0.69	2-5
Zr	180	1-5
Hf	7.6	3-5
Ta	1.34	2-6
Th	8.7	3-5
U	-	10-25

## Appendix 3: cont.

9122A: Bend pumice lapilli from the top of Green Mountain, SW1/4  
SE1/4 S14, T19S, R11E.

Uncertainties reported at a one standard deviation confidence level  
and account for accuracy in reproduction of standards and  
experimental errors.

	MAJOR ELEMENT OXIDES (%)					
	<u>734D</u>	<u>3234</u>	<u>3245</u>	<u>BHT3</u>	<u>9121A</u>	<u>8251A</u>
SiO <sub>2</sub>	72.5	74.0	74.2	-	73.4	74.7
TiO <sub>2</sub>	0.16	0.14	0.14	-	0.14	0.15
Al <sub>2</sub> O <sub>3</sub>	14.4	13.2	14.6	-	14.0	14.3
FeO	2.20	1.86	1.86	1.88	1.91	1.99
MgO	0.1	0.1	Tr	-	0.1	0.1
CaO	0.87	0.85	0.82	-	0.91	0.88
Na <sub>2</sub> O	4.7	4.8	4.6	4.8	4.8	5.1
K <sub>2</sub> O	3.5	3.4	3.6	-	3.6	3.4
TOTAL	98.5	98.4	99.8	-	98.8	100.6

	MINOR AND TRACE ELEMENTS (PPM)					
Sc	4.6	4.5	4.6	4.7	-	-
Cr	<1	<1	3	2	-	-
Co	0.53	0.51	0.52	0.60	-	-
Ni	-	1	2	1	-	-
Rb	61	81	84	70	-	-
Sr	69	66	50	60	-	-
Cs	2.7	2.9	2.9	3.0	-	-
Ba	770	990	890	840	-	-
La	29.2	30.8	30.2	30.1	-	-
Ce	59	64	66	61	-	-
Nd	26	22	23	28	-	-
Sm	6.17	6.14	6.11	6.18	-	-
Eu	0.79	0.77	0.72	0.78	-	-
Tb	0.97	0.99	1.03	1.06	-	-
Yb	4.3	4.4	4.4	4.4	-	-
Lu	0.68	0.72	0.68	0.72	-	-
Zr	-	170	170	-	-	-
Hf	6.8	7.1	7.2	8.3	-	-
Ta	1.18	1.31	1.35	1.31	-	-
Th	8.1	8.1	8.3	8.3	-	-
U	2.4	2.3	3.0	3.3	-	-

#### Appendix 4: Tumalo tuff geochemistry and sample locations

- 734D: Interior of 15 cm pumice, Tumalo tuff roadcut along Jack Pine Spring Rd, SW1/4 SE1/4 Sec 33, T17S, R11E.
- 3434: Interior of 30 cm pumice, welded Tumalo tuff exposure along Tyler Rd., NE1/4 NW1/4 Sec 2, T16S, R11E.
- BHT3: Interior of 10 cm pumice, Tumalo tuff exposure in pumice quarry, NW1/4 SE1/4 Sec 11, T18S, R11E.
- 9121A: Tumalo tuff pumice lapilli from top of unnamed cinder cone, NW1/4 SE1/4 Sec 35, T17S, R11E.
- 8251A: Interior of 5 cm grey pumice, Tumalo tuff exposure in pumice quarry, NW1/4 NW1/4 Sec 36, T18S, R11E.

## MAJOR ELEMENT OXIDES (%)

	<u>BHT1</u>	<u>BHT5</u>	<u>BHT7</u>
SiO <sub>2</sub>	-	-	-
TiO <sub>2</sub>	-	-	-
Al <sub>2</sub> O <sub>3</sub>	-	-	-
FeO	1.98	1.88	2.18
MgO	-	-	-
CaO	-	-	-
Na <sub>2</sub> O	4.52	4.56	4.56
K <sub>2</sub> O	-	-	-

## MINOR AND TRACE ELEMENTS (PPM)

Sc	4.7	4.7	4.7
Cr	2	3	2
Co	0.51	0.55	0.57
Ni	-	-	-
Rb	73	68	66
Sr	65	70	68
Cs	3.0	3.2	2.7
Ba	850	850	870
La	30.4	30.8	30.5
Ce	62	61	64
Nd	29	26	29
Sm	6.18	6.20	6.16
Eu	0.80	0.73	0.78
Tb	1.03	1.02	1.03
Yb	4.4	4.4	4.3
Lu	0.70	0.71	0.68
Zr	170	180	170
Hf	8.4	8.1	8.7
Ta	1.28	1.30	1.29
Th	8.3	8.7	8.4
U	3.5	3.3	3.3

## Appendix 4 cont.

BHT1, 5, 7, : Rhyodacitic pumice zones from 3 Tumalo tuff mixed pumice blocks, all exposed along Columbia Canal, NW1/4 NE1/4 Sec 20, T17S, R11E.

	MAJOR ELEMENT OXIDES (%)					
	753E	6291S	4172S	3245S	3235S	Unc. (%)
SiO <sub>2</sub>	74.8	73.9	74.0	75.6	74.8	2-4
TiO <sub>2</sub>	0.15	0.16	0.15	0.15	0.16	5-10
Al <sub>2</sub> O <sub>3</sub>	14.0	15.8	15.2	13.2	14.3	5-10
FeO	2.08	2.02	1.93	1.97	1.95	3-5
MgO	0.1	0.1	0.1	Tr	0.1	50
CaO	0.88	0.91	0.87	0.86	0.90	4-6
Na <sub>2</sub> O	4.7	4.4	4.4	4.7	4.5	1-5
K <sub>2</sub> O	3.6	3.4	3.8	3.6	3.8	1-5
TOTAL	100.4	100.7	100.5	100.4	100.5	

	MINOR AND TRACE ELEMENTS (PPM)					
Sc	-	4.8	4.5	4.6	4.8	1-3
Cr	-	1	1	<1	2	10-50
Co	-	0.48	0.55	0.57	0.56	5-10
Ni	-	2	4	3	1	20-50
Rb	-	78	82	81	80	8-12
Sr	-	76	71	71	62	15-35
Cs	-	2.7	2.8	2.9	2.7	5-10
Ba	-	860	860	850	780	2-6
La	-	29.8	29.7	29.8	30.5	1-2
Ce	-	62	63	65	63	1-5
Nd	-	22	37	25	24	5-30
Sm	-	6.06	6.06	6.11	6.14	1-2
Eu	-	0.78	0.74	0.77	0.82	1-2
Tb	-	1.00	1.00	1.02	1.03	1-2
Yb	-	4.2	4.2	4.3	4.4	2-5
Lu	-	0.65	0.68	0.71	0.69	2-5
Zr	-	170	170	170	170	1-5
Hf	-	7.0	6.9	7.1	7.0	3-5
Ta	-	1.33	1.46	1.33	1.31	2-6
Th	-	7.9	7.9	8.2	8.0	3-5
U	-	2.8	2.8	2.5	2.2	10-25

#### Appendix 4: cont.

753E: Rim of 10 cm altered pumice, 100 m east from sample 3245.

6291S: Rhyodacitic pumice zone from 35 cm Tumalo tuff mixed pumice, NW1/4 NE1/4 Sec 8, T17S, R11E.

4172S: Rhyodacitic pumice zone from 20 cm Tumalo tuff mixed pumice, exposure along Columbia Canal, NW1/4 NE1/4 Sec 20, T17S, R11E.

3235S: a/a, 30 cm Tumalo tuff mixed pumice.

3245S: Rhyodacitic pumice zone from 20 cm Tumalo tuff mixed pumice, exposure in abandoned pumice quarry, NW1/4 SE1/4 Sec 11, T18S, R11E.

## MAJOR ELEMENT OXIDES (%)

	<u>6291M</u>	<u>4172M</u>	<u>3245M</u>	<u>3234M</u>
SiO <sub>2</sub>	65.4	66.2	66.6	65.1
TiO <sub>2</sub>	0.88	0.95	0.91	0.89
Al <sub>2</sub> O <sub>3</sub>	17.6	16.4	16.3	17.2
FeO	5.4	5.7	5.7	5.5
MgO	1.4	1.4	1.5	1.5
CaO	3.8	3.5	3.7	3.6
Na <sub>2</sub> O	5.0	5.0	5.0	5.2
K <sub>2</sub> O	1.9	1.9	2.0	1.9
TOTAL	<u>101.2</u>	<u>101.0</u>	<u>101.6</u>	<u>100.9</u>

## MINOR AND TRACE ELEMENTS (PPM)

Sc	10.9	13.2	10.7	11.6
Cr	10	9	10	17
Co	4.4	5.1	4.4	4.7
Ni	6	8	6	10
Rb	46	45	53	50
Sr	280	340	250	280
Cs	1.6	1.7	1.9	1.6
Ba	730	750	700	750
La	27.3	28.4	27.9	27.6
Ce	57	63	62	58
Nd	30	29	34	28
Sm	7.4	8.2	7.8	7.7
Eu	1.76	2.15	1.80	1.90
Tb	0.97	1.01	1.00	0.95
Yb	4.3	4.3	4.4	4.4
Lu	0.64	0.75	0.68	0.68
Zr	150	170	160	160
Hf	5.6	6.3	6.1	5.9
Ta	1.04	1.13	1.07	1.05
Th	4.8	4.9	5.3	4.8
U	1.2	1.8	1.9	1.7

## Appendix 4 cont.

6291M: Dacitic pumice zone, same location as 6291S.  
 4172M: Dacitic pumice zone, same location as 4172S.  
 3245M: Dacitic pumice zone, same location as 3245S.  
 3235M: Dacitic pumice zone, same location as 3235S.



## MAJOR ELEMENT OXIDES (%)

	<u>BHT2</u>	<u>BHT4</u>	<u>BHT6</u>	<u>Unc (%)</u>
SiO <sub>2</sub>	-	-	-	2-5
TiO <sub>2</sub>	-	-	-	3-5
Al <sub>2</sub> O <sub>3</sub>	-	-	-	5-8
FeO	4.6	4.9	5.5	3-5
MgO	-	-	-	5-10
CaO	-	-	-	3-6
Na <sub>2</sub> O	5.0	5.1	4.8	1-5
K <sub>2</sub> O	-	-	-	3-5

## MINOR AND TRACE ELEMENTS (PPM)

Sc	12.1	13.1	11.3	1-3
Cr	12	10	14	10-30
Co	4.4	5.9	4.6	5-8
Ni	-	-	-	20-50
Rb	40	37	38	15-20
Sr	-	-	-	13-15
Cs	1.7	1.8	1.6	6-10
Ba	740	700	730	3-5
La	28.2	27.2	29.2	3-5
Ce	59	57	58	5-8
Nd	33	33	31	7-10
Sm	7.9	7.6	8.1	1-4
Eu	1.85	1.95	2.11	1-5
Tb	1.00	1.00	0.99	1-4
Yb	4.3	4.5	4.4	3-5
Lu	0.67	0.66	0.68	4-6
Zr	180	160	140	5-8
Hf	6.4	6.5	6.9	4-6
Ta	1.08	1.06	1.15	2-5
Th	4.8	4.6	5.0	4-6
U	2.3	2.4	2.3	15-20

## Appendix 4 cont.

BHT2, 4, 6: Dacitic pumice zones from Tumalo tuff mixed pumices blocks, same locations as BHT1, 5, and 7.

Uncertainties reported at a one standard deviation confidence level, and account for accuracy in reproduction of standards and experimental errors.